AD-A058 358 NAVAL RESEARCH LAB WASHINGTON D C F/G 4/1
MICROWAVE RADIOMETRIC SENSING OF THE MARINE BOUNDARY LAYER.(U)
DEC 77 C I BEARD, L U MARTIN

UNCLASSIFIED NRL-MR-3686 SBIE-AD-E000 188 NL

| OF |
AD
A058 358

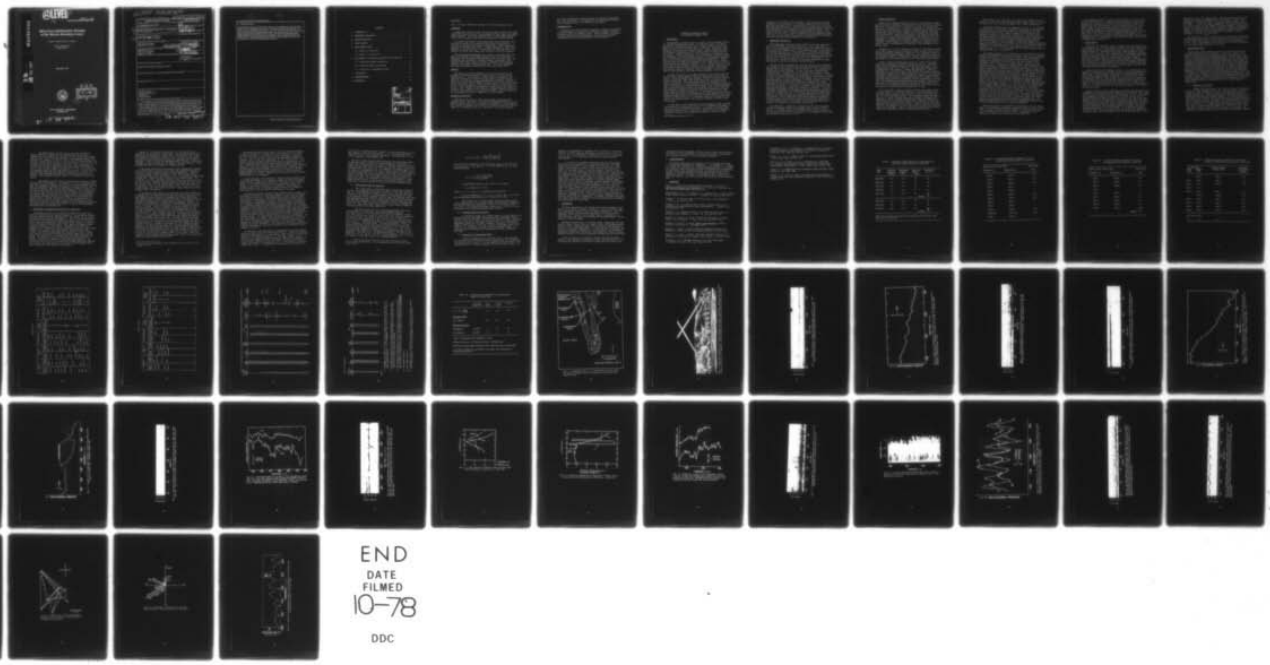

END
DATE
FILMED
10-78
DDC

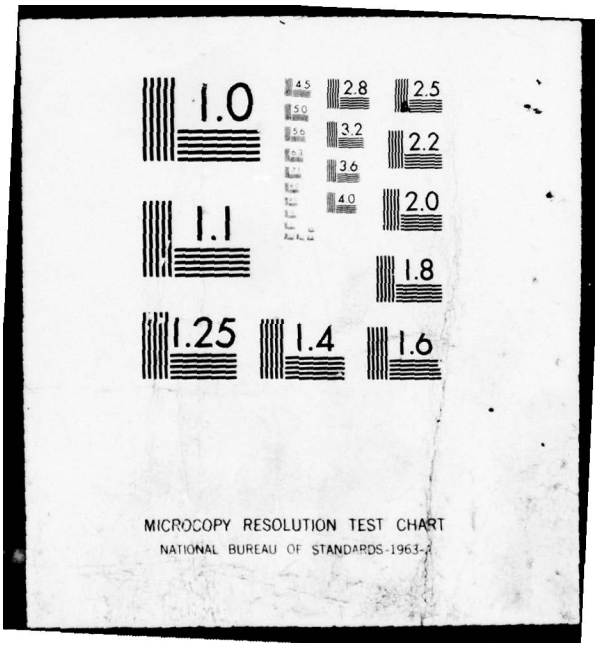
1.0
1.1
1.25
1.4
1.6
1.8
2.0
2.2
2.5
2.8
3.2
3.6
4.0
4.5
5.0
5.6
MICROCOPY RESOLUTION TEST CHART
NATIONAL BUREAU OF STANDARDS-1963-A

NRL Memorandum Report 3686

Microwave Radiometric Sensing of the Marine Boundary Layer

CHARLES I. BEARD and LEE U. MARTIN

Airborne Radar Branch
Radar Division

December 1977

NAVAL RESEARCH LABORATORY
Washington, D.C.

(18) SBIE (19) AD-E000 188

SECURITY CLASSIFICATION OF THIS PAGE (When Data Entered) (14) NRL-MR-3686

REPORT DOCUMENTATION PAGE

READ INSTRUCTIONS BEFORE COMPLETING FORM

1. REPORT NUMBER: NRL Memorandum Report 3686

2. GOVT ACCESSION NO.

3. RECIPIENT'S CATALOG NUMBER (9)

4. TITLE (and Subtitle) (6): MICROWAVE RADIOMETRIC SENSING OF THE MARINE BOUNDARY LAYER,

5. TYPE OF REPORT & PERIOD COVERED: Final Report, for FY 76 and FY 77,

6. PERFORMING ORG. REPORT NUMBER

7. AUTHOR(s) (10): Charles I. Beard and Lee U. Martin

8. CONTRACT OR GRANT NUMBER(s)

9. PERFORMING ORGANIZATION NAME AND ADDRESS: Naval Research Laboratory, Washington, D.C. 20375

10. PROGRAM ELEMENT, PROJECT, TASK AREA & WORK UNIT NUMBERS: NRL Problem R07-37 9 9; 61153N-22 & RR0210141 (16) RR02101 (17)

11. CONTROLLING OFFICE NAME AND ADDRESS: Department of the Navy, Office of Naval Research, Arlington, VA 22217

12. REPORT DATE (11): Dec[redacted]77

13. NUMBER OF PAGES: 58 (12) 59p.

14. MONITORING AGENCY NAME & ADDRESS (if different from Controlling Office)

15. SECURITY CLASS. (of this report): UNCLASSIFIED

15a. DECLASSIFICATION/DOWNGRADING SCHEDULE

16. DISTRIBUTION STATEMENT (of this Report)

Approved for public release; distribution unlimited.

17. DISTRIBUTION STATEMENT (of the abstract entered in Block 20, if different from Report)

18. SUPPLEMENTARY NOTES

19. KEY WORDS (Continue on reverse side if necessary and identify by block number)

Microwave radiometry
Atmospheric internal waves
Remote sensing
Atmospheric layers

20. ABSTRACT (Continue on reverse side if necessary and identify by block number)

An experiment in 1975 demonstrated that 22-GHz microwave radiometers could detect, and localize in altitude, long-period (3-15 min) internal gravity waves on low-level atmospheric inversion layers. A second experiment in June 1976 examined atmospheric structure in finer detail by using two 3°-beamwidth antennas. This has resulted in the first observation and correlation between microwave radiometer beams of short-period (1-2 min), Kelvin-Helmholtz waves. In addition, during slowly varying synoptic conditions, the radiometers followed changes in the height of the inversion base with an average sensitivity of 25 m/°K. Using an atmospheric "quiet period" to determine

(Continues)

DD FORM 1 JAN 73 1473 EDITION OF 1 NOV 65 IS OBSOLETE S/N 0102-014-6601

251 950

78 07 10 061

SECURITY CLASSIFICATION OF THIS PAGE (When Data Entered)

20. Abstract (Continued)

the radiometer noise level, the resulting vertical resolution of the radiometer is shown to be approximately ±1 meter, comparable to active sensors. The observed sensitivities were unaffected by the presence of stratus clouds beneath the inversion. On 19 June 1976, a 5.5-hour sequence of 10- to 11-minute period waves showed recurring internal (gravity) wave propagation from 3 or 4 directions. The corresponding radiometer undulations shifted time-phase 180° with the microbarograph surface pressure undulations when the direction of wave propagation changed. Calculation of wave phase velocities based on meteorological soundings favor 2nd mode wave propagation, in agreement with the observed wave velocities and microbarograph periodicities.

CONTENTS

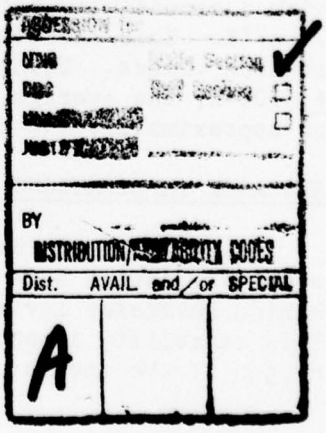

MEMORANDUM

Subj: Microwave Radiometric Sensing of the Marine Boundary Layer

BACKGROUND

Atmospheric inversion layers may cause ducting conditions and radar holes which adversely affect the performance of Navy radars and communications systems. A passive, shipborne method of detecting inversion layers would be useful, particularly during times of radio silence.

An initial experiment in 1975 demonstrated that long-period (3-15 min) gravity waves on the inversion layer could be detected and localized in altitude with microwave radiometers. These results were reported in NRL Memo Report 3283. A second experiment in June 1976 examined the inversion layer in finer detail by using two narrow (3°) beamwidth antennas whose beams could intersect at various altitudes.

The ground-based radiometers were located at San Diego where the Naval Ocean Systems Center (NOSC) (formerly the Naval Electronics Laboratory Center) provided "atmospheric-truth" for comparison to the radiometer data obtained by the Naval Research Laboratory. NOSC provided FM-CW radar, acoustic sounder, ceilometer, microbarograph, radiosonde and surface meteorological data. This report primarily describes measurements conducted from 24 May to 20 June 1976.

FINDINGS

One result of the 1976 experiment was the first detection and correlation between radiometers of short-period (1-2 min), Kelvin-Helmholtz waves. The presence of these waves was confirmed by the simultaneous detection by the FM-CW radar and/or acoustic sounder. In addition, during slowly varying meteorological conditions, the radiometer trace would follow changes in the altitude of the inversion base with a sensitivity between 17 and 100 m/°K, with an average value of 25 m/°K. This sensitivity was apparently unaffected by the presence of stratus clouds. Using a "quiet" period to measure radiometer noise at $\pm$ 0.05°K, the average 25 m/°K sensitivity yields a vertical resolution of approximately $\pm$ 1 meter, comparable to active sensors.

RESEARCH IMPLICATIONS

Analysis of the data has shown that microwave radiometers can passively detect both small- and large-scale phenomena occurring in the marine inversion layer with a sensitivity comparable to active sensors. This capability enhances their ability to passively detect and find the height of the inversion layer for calculation of ducting conditions.

The height determination requires either two separated radiometers (e.g., bow and stern), or two beams from a single shipboard station with measurements made at two different ship speeds.

RECOMMENDATIONS

Analysis of the data should be continued to explore the potential of the radiometers to measure the thickness and change of index of refraction across the inversion layer. These parameters are needed for quantitative ducting calculations; they would also markedly increase the value of the radiometers as remote sensors.

MICROWAVE RADIOMETRIC SENSING OF THE MARINE BOUNDARY LAYER

1. INTRODUCTION

The atmospheric boundary layer is a region of both internal motions and boundary interactions at micro- to meso-scale sizes. Of special interest is the marine boundary layer, a region characterized by cool moist air near the surface with warm dry air above. Separating these different air masses is an inversion layer, a narrow transition region 25-100 meters in thickness, which is located 200 to 500 meters above the surface. Typical changes are 5-10°C increases in temperature and 75% decreases of relative humidity across this stable transition region. This inversion layer is the primary location for propagating atmospheric waves, as discussed extensively by Gossard and Hooke (1975). These internal waves can affect electromagnetic wave propagation by intensifying refractivity gradients (Gossard, et. al., 1970), which in turn can cause radar "holes" (Vickers and Lopez, 1975). Internal (gravity) waves also transport momentum which affects local atmospheric circulations. One cause of clear air turbulence (CAT) is now known to be the breakdown of waves induced by wind shear (Kelvin-Helmholtz (K-H) waves).

As these waves occur at the upper boundary of the marine layer and are transitory, remote means of detection are needed to study them in detail. The active FM-CW radar (Richter, 1969) and the active acoustic sounder (McAllister, 1968) have proved very useful in detecting the waves by backscatter from small-scale humidity or temperature turbulence, respectively. A 1975 experiment by the Naval Research Laboratory (NRL) at the Naval Ocean Systems Center (NOSC) in San Diego demonstrated that long-period gravity waves on an inversion layer could be detected and localized in height using passive microwave radiometers as remote sensors (Martin and Beard, 1976a, b). At a frequency of 22 GHz, the water vapor transition, the ground-based microwave radiometers primarily measured changes caused by the waves in the column height of water vapor beneath the inversion; this is a different principle of operation from that of the active sounders, which require turbulence for their detection process.

In June 1976, a second experiment (also performed at NOSC) extended the previous NRL work by using two narrow (3°) beamwidth radiometers to study finer-scale atmospheric structure. Altitudes of the waves were determined from the cross correlation of signals from two horizontally separated radiometers whose beams were elevated to intersect above,

Note: Manuscript submitted April 3, 1978.

below and at the height of the inversion. Cross correlation between radiometers is also capable of providing information on the velocity and decay characteristics of perturbations occurring at the inversion. NOSC furnished FM-CW radar, acoustic sounder, microbarograph, ceilometer, and radiosonde data for comparison to the radiometer results. This report primarily contains results obtained during the experiment from 24 May to 20 June 1976. Section 2 describes the experimental arrangement, with the succeeding four sections describing different phenomena. The final section includes summaries and conclusions.

2. EXPERIMENT DESCRIPTION

The experimental site was located at NOSC on the west side of the Point Loma Peninsula, San Diego, California. Point Loma, shown in Fig. 1, is an approximately north-south ridge with a maximum elevation of 135 m-MSL (all heights will be above Mean Sea Level); to the west is the Pacific Ocean and to the north and east is the city of San Diego. For the 1976 measurements, two narrow beam antennas (3°) were used in place of the one wide (22°) and one narrow (3°) beamwidth (bw) antennas used in 1975. The lateral resolution of the 3° bw antennas at an altitude of 0.5 km was 25 meters, thus allowing observation of waves with lengths as short as 50 meters at this altitude.

The base station radiometer for both the 1975 and 1976 experiments was located on the roof of the same building (elevation 40 m) at the western edge of the peninsula (site S_1 in Fig. 1). The ceilometer was located next to this building. In 1975, the remote radiometer was co-located near the ridge with the FM-CW radar and acoustic sounder (altitude 105 m), resulting in an E-W baseline of 427 meters. Initially in 1976, the remote radiometer was moved farther south along the ridge to site S_3 (Fig. 1) at an altitude of 125 meters. Site S_3 provided a 965-meter baseline between radiometers in a NW-SE azimuth. On 14 June 1976, because of continuing IF interference problems, the remote radiometer was moved to a lower site on the western edge of the peninsula (site S_2 in Fig. 1 at 31 meters altitude); this provided a baseline also 965 meters in length at an azimuth of 160°-340°. This path additionally possessed the advantage of being approximately parallel to the ridge; consequently, the ridge should have the least asymmetrical effect on the path (see Fig. 2). The data discussed below were taken primarily on this last path, although some data from all three paths are included. With a separation of 965 meters between radiometers, elevation angles from 20 to 69° varied the intersection region of the two beam axes from 200 to 1250 meters to cover the expected height range of the inversion and associated wave activity.

The radiometers, essentially unchanged from the 1975 experiment, were of Dicke design and had the reference loads cooled by liquid nitrogen. One minor change was the reduction of the time constant in the low pass filter from 15 to 10 seconds. This changed the calculated rms sensitivity from 0.03 to 0.04°K.

3. HEIGHT SENSITIVITY

During slowly changing synoptic conditions, the radiometer signal would follow both increases and decreases in the height of the inversion base with a high sensitivity. This occurs because, in general, the marine air is unstable near the surface, resulting in a sufficient transfer of water vapor upwards to develop a well-mixed marine layer with uniform water content. Thus, changes in the thickness of the marine layer correspond to changes in the height of the inversion base above the surface. Since the microwave radiometer operates at 22 GHz, the frequency of the water vapor transition line, the sensitivity of the radiometers to changes in the thickness (height) of the marine air is a maximum. These changes in inversion height can be caused by atmospheric waves or strengthening or weakening of the subsidence of the dry air aloft.

Sensitivity, S, will be defined as the ratio of the change in slant path length, resulting from an inversion height change, to the corresponding radiometer temperature change ΔT, or $S = \Delta h/\Delta T \sin\psi$, where Δh is the vertical height change as measured by the FM-CW radar, and ψ is the elevation angle of the radiometer. Several examples of sensitivity measurements are discussed below, for both clear and overcast skies.

Figure 3 shows the FM-CW radar record of 12 June 1976 and Fig. 4 shows the corresponding radiometer record from site S_2. The FM-CW record shows a gradual decrease of 100 meters in the height of the inversion base from 1600 to 1700 GMT. The radiometer signal shows a corresponding 2.9°K decrease in brightness temperature. With the radiometer at an elevation angle of 60 degrees, this height change of 100 meters produces a path length change of $100/\sin 60° = 115.5$ meters. This gives a sensitivity, S, of 40 meters/°K. Table I gives details of the height and corresponding brightness temperature changes for both clear and overcast skies as observed by the two radiometers on 18 June 1976. The individual sensitivities show some scatter, in part due to uncertainty in reading the height change from the FM-CW film trace ($\pm$ 10 m), but the average sensitivity values for both clear (32 m/°K) and overcast (33 m/°K) skies are essentially the same.

On 19 June 1976, during a 70-meter decrease in the height of the inversion from 1430 to 1520 GMT (see Fig. 5 for FM-CW radar record), the skies abruptly changed from overcast to clear at 1503 GMT (see Fig. 6 for the ceilometer record). The radiometer signal from site S_2 (see Fig. 7) shows a gradual brightness temperature decrease corresponding in time to the FM-CW radar record. There is, however, no abrupt change in the radiometer signal that corresponds to the rapid transition from overcast to clear skies. Later in the day (from 1730-1833 GMT), the sensitivity during clear skies was close to the earlier values (1430-1520 GMT). Thus, on both the 18th and 19th, the stratus clouds had a negligible effect on radiometer sensitivities.

Additionally, on 19 June 1976, the sensitivities doubled over the values of 18 June 1976, both radiometers gave average values of 17 m/°K. The reason for this doubling is unknown and is under investigation.

The measured sensitivities are summarized in Fig. 8. The ordinate is $(\Delta T)(\sin\psi)$. The abscissa is $(\Delta RH)(\Delta h)$, where ΔRH is the change in relative humidity across the inversion (as determined by the NOSC radiosonde), and Δh is the change in height of the inversion (i.e., change in thickness of marine air, as measured by the FM-CW radar). The dashed line is an average drawn through the points (excluding the one at an abscissa of 90). This linear relation follows from the radiometer equation for small changes of brightness temperature, $\Delta T_B \propto \Delta\rho_v \cdot \Delta h$, where $\Delta\rho_v$ is the change in water vapor density across the inversion (from the moist to dry air), and Δh is the change in thickness of moist air. The sensitivity is the reciprocal slope of this line $(\Delta RH)(\Delta h)/(\Delta T) = 14.5$. As the average ΔRH for these data was 0.66, the average sensitivity = 22 meters/°K.

The maximum sensitivity to be expected can be estimated as follows. Assume a step decrease in the density of water vapor (ρ_v) at a height h (solid line in Fig. 9), and that an increase in inversion height by Δh increases the thickness of the underlying moist layer to yield an increase in brightness temperature T_B. Reasonable values of the parameters are h = 400 m, ρ_1 = 12 gm/m^3 and ρ_2 = 3 gm/m^3. For an increase in Δh of 40 meters, the computer model used in Martin and Beard (1976a) gives a brightness temperature increase of 0.72°K, which yields a sensitivity of 56 m/°K for a radiometer elevation angle of 45°. Clouds beneath the inversion should increase the sensitivity because of the emission from the liquid water in clouds. If the thickness of the cloud deck remains constant with changes in inversion height, i.e., the base and top of the cloud deck vary together, the net effect of the clouds is to increase the brightness temperature contrast between the moist and dry air. This will give a sensitivity larger than without clouds, but constant with time. If, however, the cloud thickness varies with inversion height changes, i.e., just the cloud top changes height, the increased sensitivity will also vary with time. In either case, ΔT will depend on Δh and the liquid water content of the clouds. Assuming a liquid water content of 0.3 gm/m^3 and Δh of 40 meters, the increase due to the clouds alone will be 0.35°K. The total temperature increase is the sum of the increases due to water vapor and liquid water, giving a net sensitivity of 37 m/°K. In reality, the decrease in water vapor will not be as sharp as described above, and, consequently, the observed sensitivities should be somewhat less. The observed average sensitivity of 22 m/°K is significantly greater than this predicted sensitivity and is being investigated.

These sensitivities (in meters/°K) were applied to several large waves in the radiometer brightness temperature trace on 18 and 19 June 1976 to convert the amplitudes into meters. The average wave amplitudes determined this way were 85% to 95%, respectively, of the average wave amplitudes read from the FM-CW radar film.

The negligible effect of stratus clouds observed on 18 and 19 June 1976 may be the result of a small liquid water content in the clouds. Observations by Ryan et. al. (1972) of the liquid water content of a stratus cloud off the California coast gave values from 0.01 to 0.35 gm/m^3 between the cloud base and top for a 300-m thick cloud. Some other possible variations of measured sensitivities are caused by (1) errors in measuring Δh from the FM-CW photographic record, (2) the FM-CW radar trace does not always correspond to the height of the inversion base since it depends on small-scale turbulence, and (3) the radiometers do not follow changes in the inversion height during rapidly changing synoptic conditions.

4. QUIET PERIODS

In general, the radiometer records indicate that the atmosphere is in constant motion. On some occasions, however, low-level winds become light enough to produce a radiometer trace so smooth that it could be called "anomalous". The FM-CW traces during these radiometer "quiet periods" are, in general, weak, intermittent, may disappear altogether, and may or may not occur at the inversion base. With weak winds, there may be insufficient shear for production of turbulence except in localized or "spotty" regions. Atlas (1969) suggested a minimum shear value of 0.01 sec^{-1}. The required combination of localized turbulence and a refractivity gradient sufficient to produce an FM-CW radar backscattered return may, therefore, occur at other heights than the inversion base and may be weak or intermittent.

A quiet period is now examined in detail, as it illustrates a difference in the mechanism of response of the two sensors (radiometer and FM-CW radar), and it provides a measurement of the radiometer noise level and a radiometer height resolution. One quiet period in the 3° bw radiometer signal is shown in Fig. 10 for 8 May 1975, a clear day. The low-level winds from the 1100-GMT Montgomery Field radiosonde were less than 0.5 m/s, and the FM-CW radar does not show a trace at the height of the inversion base (452 m) at 1300 GMT, but instead at 562 m (Fig. 11). Not until 1725 GMT did an FM-CW echo appear at the height of the inversion base.

Prior to the quiet period beginning at 1306 GMT, when the FM-CW trace disappeared, there were very small undulations on both FM-CW radar (such as those after 1440 GMT in Fig. 11) and radiometer outputs. (For comparison, examples of disturbed inversions are in Figs. 13, 17 and 20.) Although the FM-CW trace disappeared from 1306 to 1352 GMT, these atmospheric undulations continued on the radiometer output (until the calibration pulse) as the column height of water vapor apparently continued to oscillate and produce the varying brightness temperature; however, there was apparently insufficient turbulence to produce a detectable backscattered signal for the FM-CW radar. For 9 minutes thereafter (1352-1401 GMT) a weak, constant-altitude (no waves) trace appeared on the FM-CW radar, but the radiometer trace became extremely quiet, with

fluctuations of $\leq$ 0.1°K, peak-to-peak. The radiometer noise level can therefore be taken as approximately $\pm$ 0.05°K ($\Delta T_{rms} \approx 0.03$°K). The calculated noise level is 0.04°K. During the next 37 minutes (1401-1438 GMT), the FM-CW trace again disappeared; the radiometer trace was still fairly quiet, but now showed two slightly larger ($\sim$0.25°K) undulations of roughly 10-minute periods, which were probably atmospheric in origin. If, however, a worst case assumption is made that these were radiometer noise, then the upper limit of the radiometer noise is certainly $< \pm$ 0.13°K ($\Delta T_{rms} \approx 0.06$°K).

The sensitivity of the 3° bw radiometer is computed by using a 68-m inversion drop from 1200 to 1300 GMT, which caused a ΔT drop of 2.6°K. At an elevation angle of 30°, this corresponds to a sensitivity of 53 m/°K. The 3° bw radiometer noise level of $\pm$ 0.05°K thus corresponds to $\pm$ 2.5-meter height resolution on this day.

5. SHORT-PERIOD WAVES

Short-period, Kelvin-Helmholtz (K-H) waves were observed by the microwave radiometers on two occasions. As far as is known to the authors, this is the first reported detection of K-H waves and their correlation between microwave radiometer beams, and has several implications. Meteorological data and FM-CW/acoustic echoes indicate that the short-period waves were shear-induced K-H waves, whose generation, propagation, interaction and dissipation are different from previously observed long-period internal (buoyancy) waves. Study of these waves can provide information on their occurrence, persistence, amplitude, period and interaction with the stable layer in which they propagate. Knowing that K-H waves travel with the mean wind (at the altitude of the waves), the correlation time between radiometer signals can be used to calculate the altitude of the waves and to measure correlation decay lengths. Finally, observation of short-period waves implies that microwave radiometers have both the sensitivity and resolution to observe small-scale phenomena and thus may be useful for remote sensing applications.

5.1 Waves on 4 June 1976

Between 0516-0540 GMT on 4 June 1976, a train of 12 waves was recorded by both radiometers (Fig. 12). The exact times of the wave crests are listed in Table II, along with the observed time delay between radiometers. Within the accuracy of the values, there is no consistent delay between radiometer signals. This was expected as the waves were at the altitude of the intersection of the antenna beams, near the inversion base at 730 meters. The average period of the waves was 2.1 minutes, and their temperature variation was 0.25°K at site S_1 and 0.3°K at site S_3. A height sensitivity measurement made several hours after the wave train had passed gave a value of 97 m/°K. This value gives a peak-to-peak height of 24 meters for the waves. The correlation between radiometer signals of other short-period phenomena

before the wave train may also represent wave activity. Short-period waves (possibly K-H waves) are evident on the FM-CW radar return throughout this time period (Fig. 13). The height of the echo base ($\approx$730 m) agrees with the reported height of the inversion base, and the intermittent echo at 900 m corresponds to the top of the inversion. There is some difficulty in determining a wave period from the FM-CW film record; however, near 0535 GMT, a period of 2 minutes is readable, in agreement with the radiometer results. One unusual feature of the FM-CW echo is the smoothness of the echo top with the wave troughs apparently extending downward into the moist air. In addition, at 0445 GMT and 0455 GMT, there is a braided echo in the dry air at 900 meters, with a possible "eye" at the inversion height at 0506 GMT.

The NOSC radiosonde data taken at 1600 GMT on 4 June supports the generation of shear-induced K-H waves with low values of Richardson's number, R_i, where Richardson's number is given by

$$R_i = (g/\theta)(\partial\theta/\partial z)/(\partial u/\partial z)^2 ,$$

where g is the acceleration of gravity, θ is potential temperature, and u is the wind velocity. A value of ≤ 0.25 for Richardson's number is generally regarded as necessary, but not sufficient, for the generation of unstable waves. Figure 14 shows the wind speed and direction, and Fig. 15 shows the potential temperature and Richardson's number. Near 750 meters was a region of easterly winds with southwesterly winds above and below. This produced shear values > 0.01 sec^{-1} above 320 meters with a maximum value of 0.02 sec^{-1} between 735 and 845 meters. The potential temperature profile shows slightly stable air from 320-790 meters with a strong inversion (0.05°K/m) between 770 and 900 meters. Calculated values of Richardson's number give two thin layers with values below 0.25, at ~ 470 m and from 730 to 780 m. Thus conditions are favorable for the generation of K-H waves at several altitudes, with the most favorable conditions existing near 735 meters where the shear has the largest value.

The FM-CW radar showed K-H waves at 730 meters and 900 meters, excellent agreement considering time differences between the wave activity and the sounding ($\approx$10 hours). The acoustic sounder return for this time period shows a weak wave echo at a height of either 403 or 745 meters. This range ambiguity exists because the range interval being monitored was set for 275-445 meters. However, the temperature profile shows adiabatic conditions near 400 meters, making it unlikely to obtain acoustic returns from this height region. Thus, the weak wave echo is most likely from 745 meters. A readable portion of the record near 0540 GMT gives a wave period close to 2 minutes, in agreement with the radiometer and FM-CW signals. Assuming that the waves are propagating in the direction of the average wind across the shear layer at the mean wind speed, the waves propagated from 120° at 1.3 m/sec. This gives a wavelength λ = (1.3 m/sec)(126 sec) = 215 meters, the shortest wavelength observed in the data so far. Miles and

Howard (1964) derived the relationship that, for K-H waves imbedded in a layer of shear of thickness Δz, the ratio of fastest growing wavelength λ to layer thickness is 7.5. The observed waves yield Δz = 215/7.5 = 29 meters, compared with the deduced radiometer peak-to-peak amplitude of 24 meters.

5.2 Waves on 17 June 1976

On 17 June 1976, from 1919 to 1932 GMT, a train of 9 waves with an average period of 1.5 minutes was observed by both radiometers, whose beams were elevated 45° and pointed toward each other in azimuth (Fig. 16). The times of the (warm) crests observed by each radiometer are listed in Table III. The time differences in the last column average 0.8 minute, with the signal from radiometer at site S_1 lagging that from site S_2. After 1932 GMT, interference appeared on the radiometer at site S_1, but the wave train continued at site S_2 (Table IV).

From the NOSC sounding (2017 GMT, 17 June 1976), conditions were again favorable for shear-induced waves. A precipitous drop in moisture beginning at a height of 416 m is assumed to be the inversion base. Just below, there was a 73° change in wind direction (from 278 m to 404 m); in this region the shear was 0.035 sec^{-1}, and Richardson's number (R_i) was 0.27, close to the critical value of 1/4. From 404 m to 519 m, the shear was still 0.027 sec^{-1}. During the 13-minute wave train (1919-1932 GMT), the FM-CW radar trace (Fig. 17) is blurred on the film (because of intense short-wave activity). Also, the acoustic sounder film (Fig. 18) is blank from 1900 to 1928 GMT; however, just afterward (until 1946 GMT) troughs of sharp, saw-tooth waves are visible. (The wave peaks are off the top of the film.) These waves are similar to the herring-bone type structure observed by McAllister, et al. (1969) during strong wind shear across a temperature inversion, and identifies them as K-H waves.

The times of the waves recorded by the acoustic sounder and radiometer are listed in Table IV. The average acoustic sounder period of 2.0 min is to be compared with the radiometer trough period of 2.1 min and the radiometer crest period of 1.9 min. The latter two should be the same, and their average of 2.0 minutes is the exact acoustic sounder period. The time lag of radiometer troughs to acoustic sounder troughs (last column in Table IV) of -0.5 ± 1.3 minutes is more erratic than the variability between the two radiometer signals (Table III); however, the variability of $\pm$ 1.3 minutes is still within one wave period. As the individual waves of the two radiometer signals show differences in shape arising during the travel time over the 200-meter beam separation distance (at the inversion height), it is to be expected that greater shape distortions will occur in the approximately 600-meter distance (along the wind direction) between the midpoint of the radiometer path and the acoustic sounder location.

The second feature of this case is the time correlation between radiometer signals and the height-finding implications. A comparison of the observed and computed lag times is now made assuming that the waves travel with the mean wind. The radiometer beams, both elevated 45°, intersect at 518 m. From the 2017 GMT NOSC sounding, the relative humidity drops from 85% at 416 m altitude to 32% at 439 m. The altitude of the waves is assumed to be 416 m. From the geometry, the two beam axes are 200 m apart where they pass through the 416-meter level. From the NOSC sounding, the wind at 404 m is 4.1 m/s from 190°; its component along the 160° path azimuth is 3.6 m/s. At this velocity, the 200-meter beam separation distance corresponds to a lag of 0.9 minutes, which compares reasonably well with the observed lag of 0.8 minutes. The wavelength along the path $\lambda \cong (3.6 \text{ m/s})(1.5 \times 60) \cong 325$ meters.

This example with K-H waves illustrates the principle of height finding with the radiometers. For example, if the two radiometers had next been elevated a different amount (or if a third radiometer beam had been in simultaneous operation to intersect the beam of site S_2 at a different elevation angle, in the same azimuth, however), then a different correlation lag time would have been obtained. From the geometry and the two lags, one can solve for the two unknowns, the altitude and the internal wave velocity in the vertical plane of the radiometers. (See Martin and Beard (1976b) for an example of this procedure using gravity waves.) Another radiometer at site S_1, but pointed 90° in azimuth from the site S_1 to site S_2 path, would presumably provide a time lag to solve for the velocity component in the orthogonal direction (as the altitude had already been found). A test of this orthogonal measurement has not been made yet.

6. THE UNUSUAL 5.5-HOUR WAVE ACTIVITY OF 19 JUNE 1976

An internal wavetrain of 5.5 hours in duration on 19 June 1976 attracted attention by the unusual behavior of the radiometric temperature fluctuations shifting time-phase 180° with respect to the microbarograph surface pressure perturbations. That is, for several periods of the 10- to 11-minute period waves, the (warm) crests of the radiometric brightness temperature fluctuations would coincide in time with the microbarograph pressure crests. Then, usually following a short transition interval of a few minutes, the phase would shift 180°, resulting in the temperature crests coinciding in time with the pressure troughs. After several more wave periods, the phase would again reverse, this sequence alternating for the entire 5.5 hours. During this time the two radiometer beams were pointed toward each other in azimuth and elevated 35° to intersect near the inversion base at 409 meters. The observed radiometer signals from the two sites were strongly correlated in time and of unusually large magnitude. The obvious question was what was causing this shifting time-phase and what did it mean? The first step was to calculate wave propagation directions and speeds to determine the time delays.

Figures 19, 20, 21 and 22 show portions of the wave activity observed by the radiometers, FM-CW radar, acoustic sounder and surface meteorological instruments, respectively. The observed times of the wave crests and troughs are listed in Table V for each of the sensors, including the phase difference between the radiometer and the microbarograph. Figure 23 shows the Montgomery Field 1100 GMT, 19 June 1976, sounding that was recorded near the middle of the wave activity. This sounding was used in the absence of an NOSC sounding.

To determine the direction and speed of wave propagation, constructions of the orbital velocity vectors were made using oscillations of the surface wind* following Gossard and Munk (G&M)(1954). Table VI lists the extremes of the excursions in the wind direction and the corresponding wind speeds (excursions in Fig. 22 are marked corresponding to Table VI). Figure 24 shows a section of the constructions. To illustrate, Pt. 28 is obtained by drawing on Fig. 24 a vector from 313° and 2.6 m/s long. Then for the next excursion extreme (Pt. 29), a vector from 344° and 4.4 m/sec long is drawn. The wind perturbation due to the wave, (2 Δu), is the vector drawn from Pt. 28 to Pt. 29. In a similar manner, the other points are drawn. These values are given in columns 5 and 6 of Table VI.

To resolve the 180° ambiguity in direction, G&M (1954) adopted the convention that the direction of the wind perturbation under the pressure maximum is the direction of propagation of the internal wave. (One minute should be subtracted from the times of the wind oscillation extremes to compare with the microbarograph crests and troughs. In addition, the tolerances in reading are $\pm$ one minute.) Thus, Pt. 30 at the 1136 GMT wind peak corresponds to the microbarograph pressure crest at 1133 GMT. Note that pressure increases downward in Fig. 22. The wind perturbation vector (from Pt. 29 and ending under Pt. 30) of 208.5° therefore is the direction of the internal wave for this oscillation, etc. Note, however, from Fig. 24 that the next perturbation, 30 to 31, suddenly changes direction. This marks the transition between an in-phase and an out-of-phase relation between radiometer and microbarograph signals (Table VI). The next three wind perturbations, 31 → 32, 32 → 33, and 33 → 34, are in approximately the same orientation, and the radiometer and microbarograph outputs are 180° out of phase (Table V). However, perturbation 34 → 35 changes direction radically, and marks the transition to an in-phase relation between radiometer and microbarograph (Table V). This in-phase relation persists until the microbarograph low at 1248 GMT, except for the one low at 1229 GMT, at which time a small change (35°) of orbital velocity direction occurred without causing a shift of the phase. This is an exception to the observed general pattern that a shift in wave direction caused the relative phase to shift 180°.

---

* The wind vane and anemometer were located at site S_1 (Fig. 1) at a height of 55 m.

The internal wave directions derived from the wind perturbations are listed in Table VI. A polar plot of the frequency of occurrence of these directions, divided into 10° class intervals, is given in Fig. 25. There are at least three main wave propagation directions (labeled as I, II, and III, arbitrarily) of 235°, 295° and 005°. Previously, Gossard and Sweezy (1974) had reported a sudden shift in the wave propagation direction following a frontal passage through the area. On 19 June 1976, however, these several directions kept recurring throughout the 5.5-hour duration of the wave train. These groups of waves propagating from different directions are similar to the wave groups (trains) of short-period internal waves in the sea found by Brekhovskikh et al. (1975). However, this is the first time they have been observed in the atmosphere.

In many instances, the "transition" regions between different wave directions are evident in the radiometer signal by either the appearance of an extra undulation in addition to the basic 10- to 11-minute period, or by a shift in phase of the two radiometer signals with respect to each other (see Fig. 19 at 1138 GMT). Little delay is expected between the two radiometer signals because the predominant wave direction of 235° is only 15° from normal to the path.

The FM-CW and acoustic sounder traces generally moved together, but they missed detecting 2 of the major changes in internal wave propagation direction (out of 9). The radiometers, however, detected every major shift in internal wave direction (signaled by the 180° shifts). This behavior is presumably a result of the differences in response of the sensors; the radiometer T_B responds to the varying column height, i.e., pressure change, and thus should correspond closely to the microbarograph pressure variations for the fundamental mode. For the 22-GHz radiometer, the varying part of the water vapor column height corresponds primarily to the lowest portion of the inversion layer containing the large drop in water vapor. The drier air above causes little response, and the well-mixed column below the inversion provides a relatively constant signal. For higher modes, the situation may be different. For the second mode, for example, the pressure perturbation in the lowest part of the inversion is of opposite sign to that at ground level as measured by the microbarograph. [See Fig. 13 of G&M, 1954.] Thus, although the 22-GHz radiometer T_B is correlated with the microbarograph pressure perturbations, the sign (or phase) of the correlation may be opposite (or 180°).

In addition to wind directions, the magnitudes of the wind perturbations (orbital winds) are obtained from Fig. 24. These are converted into phase velocities (C_i) of the internal waves relative to the moving medium by the "impedance equation," $C_i = \frac{\omega}{k} = \frac{\Delta p}{\rho \Delta u}$, where ω is the intrinsic wave angular frequency relative to the drifting medium, k is the horizontal component of the wave number, Δp and Δu are observed pressure and velocity perturbations, and ρ is the density of the atmosphere (G&M (1954)). A representative value from the calculations is

$C_i \cong 2$ m/s. The phase velocity relative to the ground would be C_i plus the component of the mean wind along C_i. For the predominant wave direction of 235°, this component was small. This magnitude of 2 m/s will be compared to calculations next.

Because of these observed phase reversals, discussed above, calculations were made of possible 2nd mode propagation. Suspicions of higher mode propagation are also raised by the shifting phases of multi-layered echoes in the drier air above the inversion layer, as shown in the FM-CW radar film in Fig. 20. For example, the topmost layer (≈ 0.65 km height) is approximately 135° out of phase with the 1125-GMT crest in the inversion layer (0.41 km height), almost 180° out at the 1143-GMT inversion trough, but back in phase at the 1157-GMT inversion trough. Later at the 1223- and the 1236-GMT inversion troughs, the phase is almost 180° again. The radiometer is relatively insensitive to these higher multiple layers in the dry air, and responds primarily to the large drop in moisture across the lowest part of the inversion layer.

6.1 Three-layer model calculations

The 3-layer model of G&M (1954) with no shear was followed as a guide. The Montgomery Field (MYF) 1100 GMT, 19 June 1976, sounding (Fig. 23) occurring near the middle of the 0830 to 1410 GMT wave train was used in the absence of an NOSC sounding. (Although MYF is 11 km to the northeast of the radiometer site at NOSC, the nighttime (1100 GMT) MYF soundings have been found to compare reasonably well with existing 1600 GMT NOSC soundings.) From the sounding, the wind shear was less than 0.006 sec^{-1} below 666 m, and increased to 0.011 sec^{-1} between 666 and 932 m. Thus, G&M's (1954) model with no shear should be adequate for the altitudes of interest below 533 m.

The entire moist layer up to the inversion base (409 m) was superadiabatic ($\approx$ -13°C/km), and the Brunt-Vaisala frequency $N = [(g/\theta)(\partial\theta/\partial z)]^{1/2}$ for this layer (N_1) would be imaginary. Therefore, the vertical wave number for this moist layer (n_1) was arbitrarily set equal to zero. For layer 2, 409 m to 533 m, $N_2 = 0.048$ sec^{-1}. Layer 3 will be considered to be from 533 m to 1513 m, with an average $N_3 = 0.019$ s^{-1}. Following G&M (1954), it is arbitrarily assumed that N_3 is constant to infinite height. The angular frequency ω for an observer drifting with the wind should be corrected for the wind ($\bar{U}$) along the wave propagation direction according to: $\omega = \Omega - \bar{U}k$, where Ω is the observed (angular) frequency in fixed coordinates, and k is the horizontal wave number $2\pi/\lambda$. Because the component $\bar{U}$ is small, it is neglected. From G&M (1954), the dispersion relation, $n^2 = k^2[(N^2/\omega^2)-1]$, yields $n_2 = k(4.71)$ and $n_3 = k(1.62)$, by approximating ω with Ω as they did (where $\Omega = 0.01$ sec^{-1} for 10- to 11-minute periods).

Thus n_2 and n_3 are real for $\omega_2 < N_2$ and $\omega_3 < N_3$, and the wave solutions are trigonometric. G&M's eigenvalue eq. (16) for the three-layer case is:

$$n_2 \cot n_2 (2\Delta H) \cong \frac{-\gamma_3\gamma_1 \coth \gamma_1 h + n_2^2}{\gamma_3 + \gamma_1 \coth \gamma_1 h} ,$$

where $2\Delta H$ is the thickness of the transition layer in their notation, $\gamma_3 = n_3$, and $\gamma_1 = -in_1$, where $n_1 \to 0$. In the limit as $n_1 \to 0$, this equation becomes:

$$n_3 + 1/h \cong \frac{n_2 - (n_3/n_2)(1/h)}{\cot n_2 (2\Delta H)}$$

An approximate solution (with $2\Delta H$ = 124 m) yields:

$$\tan (590k \pm q\pi) = 0.78,$$

where q = 0, 1, 2, etc., to accommodate multiple modes.

For the fundamental, q = 0, $k_o \cong 1.13$ km^{-1}, and $\lambda_o \cong 5.6$ km. The corresponding phase velocity $C_o = (\Omega/2\pi)\lambda_o \cong 8.9$ m/s.

This velocity is 4.5 times larger than the average value of 2 m/s calculated from the wind and pressure perturbations. Therefore, the 2nd mode values are calculated. For q = 1, $K_1 \cong 6.5$ km^{-1} and $\lambda_1 \cong 1.0$ km. The corresponding phase velocity $C_1 = (\Omega/2\pi)\lambda_1 \cong 1.5$ m/s, calculated from the wind and pressure perturbations.

6.2 Two-layer model calculations

A calculation using the two-layer model is a quick check on the fundamental (only) wavelength calculated from the three-layer model. From eq. (16b) of G&M (1954), $C^2 \cong gh\Delta(\ln\theta)$, where h = 409 m, the inversion base, and $\Delta\ln\theta$ is the change in the natural log of the potential temperature across the 124-meter thickness. From this, C ≅ 10.8 m/s. Using $\Omega = 10^{-2}$ rad/sec, $\lambda \cong 6.7$ km. This is a reasonable check of the value for the fundamental obtained from the three-layer model. As $n_2(2\Delta H)<1$, the two methods should approximately agree, according to G&M (1954).

6.3 Discussion of propagation modes

Table VII summarizes the calculated values. The wavelength and phase velocities calculated from the pressure and wind oscillations are too small (by a factor 1/4.5) when compared with the values of the fundamental mode, but agree reasonably well with 2nd-mode values. In

addition, the wavelength to thickness ratio ($L/2\Delta H$) of 8 for the 2nd harmonic is larger than any calculated by various models (7.85, 6.5, 4.9, 4.5, etc.) as summarized by Gossard (1974), but it does approximate the value of 10 calculated from observed wind and pressure fluctuations.

If the 10- to 11-minute period waves are the 2nd harmonic, then where is the fundamental? According to Table VII, the fundamental period would be 4.5 times longer (3-layer model) or 5 times longer (2-layer model); either of these would be very difficult to detect in the signal record. Clues are apparent, however, in the plot (Fig. 26) of microbarograph pressure highs (Δp's), measured from the running average. Each high (Δp) is a circled point, and the points are connected by dashed lines merely for clarity of the modulation periodicity. The plot shows a clear-cut periodic modulation of these crests with seven consecutive periods of 41-minute average length. (One crest at 1333 GMT is ill-defined, possibly because of distortion from the usually large and inaccurate peak at 1253 GMT.) This periodicity may represent the "missing" fundamental; it is 4 times the observed period, compared to the three-layer model prediction of 4.5 times. In addition, all (except one) of these crests (from the running mean) are only 55 microbars or less, whereas Table 2 of G&M (1954) shows Δp's averaging 0.18 mb (180 μbars), about 3 times these values. These small observed Δp's of $\leq$ 55 μbars are also consistent with a 2nd harmonic rather than the fundamental. In summary, although surprising, the various parameters in Table VII favor the existence of 2nd harmonic wave propagation on 19 June 1976.

7. CONCLUSIONS

The first experiment in 1975 showed that 22-GHz radiometers could detect, and localize in height, long-period (3-15 min) internal waves on an atmospheric inversion layer in a marine environment. The 1976 experiment showed that much finer atmospheric structure could be observed with two narrow (3°) radiometer beams. An example is the first detection, and correlation between two radiometer beams, of short period (1-2 min) K-H waves.

Radiometer sensitivities to inversion height changes were the same whether a solid stratus layer was present or not, and averaged approximately 25 m/°K, a sensitive value. With radiometer noise measured at $\pm$ 0.05°K, this yields approximately $\pm$ 1 meter vertical resolution, thus making the radiometer comparable to active sounders. The radiometric temperature undulations, converted by the sensitivity factor to meters, compared favorably to the wave amplitudes obtained from the FM-CW radar.

A train of long (10- to 11-minute) period waves showed unusual behavior. The radiometer undulations shifted time-phase 180° with the microbarograph pressure fluctuations at times when the internal wave

propagation directions changed. Three or four principal wave directions were found to recur throughout the 5.5-hour wave train. Calculations and observations seemed to favor second mode propagation.

8. ACKNOWLEDGMENTS

The authors appreciate the assistance of the following NRL people in building and installing the radiometers: G. W. Hermann, B. E. Kremer, A. D. Long, and F. Sollner, Jr. Special appreciation goes to F. Sollner for devising a simple and effective means of preventing the condensation of water vapor on the radiometer lenses. The authors are also very grateful to the NOSC personnel for providing data from their array of atmospheric sensors. Of these, V. R. Noonkester and W. Horner were especially helpful, the latter providing the voluminous balloon sounding data.

9. REFERENCES

Atlas, D., "Clear Air Turbulence Detection Methods: A Review," in Clear Air Turbulence and Its Detection, Y. H. Pao and A. Goldburg, eds., pps. 381-401, Plenum Press, New York, 1969.

Brekhovskikh, L. M., K. V. Konjaev, K. D. Sabinin and A. N. Serikov, "Short-Period Internal Waves in the Sea," J. Geophys. Res., 80, 856-864, 1975.

Gossard, E. E. and W. H. Munk, "On Gravity Waves in the Atmosphere," J. Meteor., 11, 259-269, 1954.

Gossard, E. E., J. H. Richter and D. Atlas, "Internal Waves in the Atmosphere from High Resolution Radar Measurements," J. Geophys. Res., 75, 3532-3536, 1970.

Gossard, E. E., "Dynamic Stability of an Isentropic Shear Layer in a Statically Stable Medium," J. Atmos. Sci., 31, 483-492, 1974.

Gossard, E. E. and W. B. Sweezy, "Dispersion and Spectra of Gravity Waves in the Atmosphere," J. Atmos. Sci., 31, 1540-1548, 1974.

Gossard, E. E. and W. H. Hooke, Waves in the Atmosphere, Elsevier Scientific Publishing Co., Amsterdam, 1975.

Martin, L. U. and C. I. Beard, "Microwave Radiometric Detection of Atmospheric Internal Waves," NRL Memorandum Report 3283, May 1976a.

Martin, L. U. and C. I. Beard, "Microwave Radiometric Detection of Atmospheric Internal Waves," Geophys. Res. Letters, 3, 327-330, 1976b.

McAllister, L. G., "Acoustic Sounding of the Lower Troposphere," J. Atmospheric Terrest. Phys. 30, 1439-1440, 1968.

McAllister, L. G., J. R. Pollard, A. R. Mahoney and P. J. R. Shaw, "Acoustic Sounding - A New Approach to the Study of Atmospheric Structure," Proc. IEEE, 57, 579-587, 1969.

Miles, J. W. and L. N. Howard, "Note on a Heterogeneous Shear Flow," J. Fluid. Mech., 20, 331-336, 1964.

Ryan, R. T., H. H. Blau, Jr., P. C. von Thuna, M. L. Cohen and G. D. Roberts, "Cloud Microstructure as Determined by an Optical Cloud Particle Spectrometer," J. Appl. Meteor., 11, 149-156, 1972.

Richter, J. H., "High Resolution Tropospheric Radar Sounding," Radio Science, 4, 1261-1268, 1969.

Vickers, W. W. and M. E. Lopez, "Low-Angle Radar Tracking Errors Induced by Non-Stratified Atmospheric Anomalies," Radio Science, 10, 491-505, 1975.

Table I. Radiometer height-sensitivity measurements for clear and overcast skies on 18 June 1976

Time GMT	Inversion change Δh (meters)	Radiometer change ΔT (°K)	Elevation angle ψ (deg.)	Sensitivity (m/°K)
0830-0935	-43	-2.9	35	26
0935-1055	+53	+2.3	35	40
1055-1200	-53	-2.0	35	46
1200-1255	-47	-3.0	35	27
1255-1500	-50	-3.0	35	29
			Average	33
2120-2150	-30	-1.6	45	27
2220-2245	-30	-2.1	30	28
2250-2310	+40	+2.0	30	40
			Average	32

First five rows are for overcast sky conditions and the last three rows are for clear skies.

Table II. Correlation between radiometers S_1 and S_3 of short-period wave train on 4 June 1976

Times of wave crests (GMT)		Lag (S_1-S_3)
Radiometer S_1	Radiometer S_3	Min.
0516.0	0516.5	-0.5
0518.0	0518.7	-0.7
0521.0	0521.5	-0.5
0523.0	0523.0	-
0524.5	0524.5	-
0526.5	0527.0	-0.5
0529.0	0528.5	+0.5
0531.0	0531.0	-
0533.5	0533.5	-
0535.5	0536.0	-0.5
0538.0(S)	0537.5(S)	+0.5
0539.5	0539.5	-

Table III. Correlation between radiometers S_1 and S_2 of short-period wave train on 17 June 1976

Times of wave crests (GMT)		Lag (S_1-S_2)
Ratiometer S_1	Radiometer S_2	Min.
1919.4	1918.6	0.8
1920.5	1919.5	1.0
1921.8	1920.9	0.9
1923.5	-	-
1925.5	1924.5	1.0
1927.6	1927.2	0.4
1929.1	1928.3	0.8
1930.8	1930.3	0.5
1932.6	1931.6	1.0
	Average	0.8

Table IV. Correlation between radiometer S_2 and acoustic sounder of short-period wave train on 17 June 1976

S_2 Radiometer Crests (GMT)	S_2 Radiometer Troughs (GMT)	Acoustic Sounder Troughs (GMT)	Lag (min) (S_2-Acoustic) S_2 Troughs
	1929.0	1929.4	-0.4
1933.4	1931.0	1932.2	-1.2
1934.6	1932.6	1934.0	-1.8
1936.2	---		
1938.5	1935.0	1935.4	-0.4
	1937.2	1938.3	-1.1
1941.3	1939.6	1940.7	-1.1
1943.0	1941.8	1941.5	+0.3
1945.1	1943.8	1943.2	+0.6
1946.8	1946.0	1945.7	+0.3
Avg. Period (min)			
1.9	2.1	2.0	

Table V

Times of crests and troughs for 19 June 1976 wave train as observed by four sensors.

Radiometer S_1		Radiometer S_2		Microbarograph		Phase Difference	FM-CW Radar		Acoustic Sounder	
Crests (warm)	Troughs (cold)	Crests (warm)	Troughs (cold)	Crests (high)	Troughs (low)	Radiometer - Microbarograph	Crests	Troughs	Crests	Troughs
		0839			0839	180°	0840.5		0841	
			0844	0842		↓				
		0847(S)			0846			0846.5		0846
0851.5		0851		0851		0°	0851		0851	
	0855		0854			--		0856		0857.5
0900.5		0859.5			0859	180°				
	0904(S)		0904	0903		↓	0902.5		0902	
0905(S)										
	0907							0906.5		0907
0911		0910.5			0910			0912		
			0913.3(S)	0912.5		↓		↑	0913(S)	
		0914.7(S)				--				
			0916.5(S)			--		Almost		
		0922			0920	180°		constant		0921(S)
			0928.5	0926		↓		height	0925(S)	
								↓		0928.5(S)
		0932			0932					
	0941.5			0939		↓			0936(S)	
			0944(S)			Transition				0942(S)
0945		0945.5(S)				--		↓	0944	
	0948.3		0947.3		0947.5	0°		0947		0949
0953		0954		0955		↓	0952		0952.5	
	1002				0957.5			0955.5		0957
						Transition	0959		0959.5	
			1006	1005		180°		1004		1005

Table V (cont.)

Radiometer S_1		Radiometer S_2		Microbarograph		Phase Difference	FM-CW Radar		Acoustic Sounder	
Crests (warm)	Troughs (cold)	Crests (warm)	Troughs (cold)	Crests (high)	Troughs (low)	Radiometer - Microbarograph	Crests	Troughs	Crests	Troughs
1009		1008.5				--	1009		1011	
	1012.3		1013			--		1014		
1015		1015			1017	180°				1016
	1020.5		1021	1021			1021		1022	
1028.5		1028			1027			1029(S)		1028(S)
	1032		1031.5	1032			1032(S)			
1036		1035			1036			1034(S)		
				1039		--	1040		1041(S)	
					1042	--		1045		
	1048		1047.5	1048		180°				1047(S)
1052		1051.5				Shifting	1051			
	1057.3		1058		1059	(0°)			1058.5	
				1104		--		1103(S)		1103
1008		1108			1107(S)	(180°)	1110		1110.5	
	1113.5		1115.3					1116.5		1116.5
1121.7		1122.7		1120		0°	1125		1123	
	1128		1129		1127			1130		1131
1133.7		1133.5		1133			1133.5		1134	
	1138.7	1137.7			1139	Transition		1137		1137.5
						--	1139.5		1139.5	
			1143	1143		180°		1142.5		1143
1148.3		1149			1148		1149.5		1150	
								1152(S)		
			1156.5	1156(S)			1153.5 (S)			1157
	1157.5				1157(S)	0°		1157		
1203.5		1204		1203			1203		1203	

Table V (cont.)

Radiometer S_1		Radiometer S_2		Microbarograph		Phase Difference	FM-CW Radar		Acoustic Sounder	
Crests (warm)	Troughs (cold)	Crests (warm)	Troughs (cold)	Crests (high)	Troughs (low)	Radiometer-Microbarograph	Crests	Troughs	Crests	Troughs
	1209.5		1210		1208	0°		1208		1208.5
1214.5		1216.5		1213		↓	1213.5		1213.5	
	1220		1220		1220	↓		1218.5		1218.5
						↓	1221		1221.5	
1225				1224		↓		1223	off film	
	1228	1228.7			1229	?			↓	
1231.3				1234		0°	1231		↓	
	1237.5		1236.5		1237.5	↓		1236	↓	1237
1242		1242.7		1242.5		↓	1243		↓	
	1248.5		1249.7		1247.5	↓		1250	↓	1249.5
1252(S)						--			↓	
	1253.7			1253		180°	1253.5		↓	
		1254.5				--			↓	
			1259.5		1300	0°		1257	↓	1256.5
1302.3		1302				--	1302		↓	
	1305.3					--			↓	
			1307(S)			--		1307.5	↓	1306
		1308.3(S)				--	1310.5		1310.5	
			1313	1314		180°		1315		1315
1321		1320.7			1321(S)	↓	1320.5		1319.5	
	1324		1326	1325(S)		↓		1326	off film	1326
1329		1330			1327(S)	↓	1331		↓	
	1336.3		1335.7	1333		↓		1336	↓	1336
1339					1337.5	↓			↓	
		1341		1342		0°	1341		↓	

Table V (cont.)

Radiometer S_1		Radiometer S_2		Microbarograph		Phase Difference	FM-CW Radar		Acoustic Sounder	
Crests (warm)	Troughs (cold)	Crests (warm)	Troughs (cold)	Crests (high)	Troughs (low)	Radiometer - Microbarograph	Crests	Troughs	Crests	Troughs
	1344					--			off film	
1348(S)					1347.5	180°		1346		1346
	1349.5(S)		1349			--				
1351(S)		1351(S)				--	1351			
			1352.5			--				
	1354.5	1353.5(S)		1354(S)		?				
			1356.3		1356(S)	0°		1356.5		1356
1359.5		1400.5		1402.5			1401			
	1405		1406		1407.5			1406		1406
1409.5		1409.5(S)		1412			1410			

Table VI. Directional peaks of surface wind oscillations; wind speeds; wind perturbations; 19 June 1976.

Arbitrary Point Number	Time (GMT)	Wind Direction	Wind Speed M/Sec	2Δu Direction	2Δu Speed M/Sec	Directional Group	Phase (Radiometer-μbarograph)	Comments
1	0918	360	3.2				180°	
2	0927	315	3.5	253	2.6	I	↓	
3	0932	352	2.9	081	2.1	I	↓	
4	0937	320.5	2.6	234	1.5	I	↓	
5	0939	350	2.2	082	1.2	I	↓	
6	0941	333	4.0	316	2.0	II	transition	
7	0944	343.4	2.2	142.5	1.9	II	↓	
8	0947	324	3.1	290.5	1.3	III	0°	
9	0953	356.3	2.6	088	1.6	I	↓	Note 1
10	0956	348	3.6	328	1.1	II	↓	
11	0959	352.4	2.5	168.5	1.1	↑	transition	
12	1001	340	2.3	235	0.6	small Δu	↓	Note 2
13	1006	350	3.7	007	1.4	↓	180°	"
14	1010	314	2.4	211	2.2	I or IV	--	"
15	1014	003	2.2	075	2.0	I	--	
16	1020	312	3.1	267	2.4	I	180°	
17	1023	320	3.6	356	0.7	↑	↓	
18	1025	315	3.6	223	0.3	very small Δu	↓	
19	1027	323	3.1	097	0.7	↓	↓	
20	1033	312	2.6	183	0.7	II	↓	Note 3
21	1038	334	1.6	011	3.7	II	↓	
22	1042	308	1.7	225	3.5	I	↓	
23	1049	344	2.2	054	3.6	I	↓	
24	1056	323	1.4	205	2.7	IV	(0°)shifting	
25	1101	347	2.0	020	4.1	IV	↓	
26	1107	326	1.4	237	3.9	I	(180°)	
27	1113	356	2.0	072	3.9	I	↓	
28	1118	313	2.6	230	3.1	I	↓	
29	1130	344	4.4	027	2.4	IV	0°	
30	1136	323	3.4	209	1.7	IV	↓	
31	1139	348	3.1	077	1.4	I	transition	
32	1147	315	2.6	224	1.7	I	180°	
33	1152	359	3.9	041	2.7	I	↓	
34	1158	308	3.1	231	3.1	I	↓	
35	1200	320	4.1	352	1.3	II	0°	
36	1203	317	3.2	150	0.9	small Δu	↓	Note 4
37	1208	332	3.8	020	1.1	II	↓	Note 5
38	1215	317	3.9	229	1.0	I	↓	

Table VI. Continued.

Arbitrary Point Number	Time (GMT)	Wind Direction	Wind Speed M/Sec	2Δu Direction	2Δu Speed M/Sec	Directional Group	Phase (Radiometer-μbarograph)	Comments
39	1222	010	4.1	070	3.5	I	0°	
40	1230	316	4.0	250	3.7	I	↓	
41	1236	005	2.0	105	3.0	III	↓	Note 6
42	1239	321	3.9	291	2.8	III	↓	"
43	1248	353	3.0	093	2.0	I or III	↓	
44	1250	332	3.0	245	1.1	I	--	
45	1252	001	3.6	055	1.7	I	--	
46	1259	322	3.0	236	2.2	I	0°	
47	1307	002	2.6	085	1.9	I	--	
48	1311	349	2.8	291	0.7	III	--	
49	1312	359	2.6	113	0.5	III	180°	
50	1316	333	3.3	293	1.5	III	↓	
51	1330	023	3.6	082	2.9	I	↓	
52	1335	343	2.8	353	2.3	I	↓	
53	1341	351	4.1	007	1.4	II	0°	
54	1345	335	2.5	193	1.9	II	--	

Notes:

1) Presumably, the "Type" of Δu (like III or I) should be the same for both lines 8 & 9 in the 0°-phase interval. On this assumption, either Type III on line 8 or Type I on line 9 then is incorrect.

2) The wind fluctuations in the interval 0959 to 1006 (points 11 to 13) are very small, and therefore the values of Δu are uncertain (both magnitude and direction), and the "Type" is not reliable and should be deleted.

3) Point 20 may be "contaminated" by the low Δu's of lines 17 to 20 and then the Δu from 19 to 20 listed on line 20 may be in error. This statement is again based on the assumption that the "Type" of Δu should be the same (such as Type I) for the entire 180°-phase interval.

4) Same comment as Note 2.

5) Same comment as Note 3.

6) Presumably, lines 41 and 42 should both be Type I to maintain the same Type throughout the 0°-phase interval. This is the same assumption as stated above in Note 1.

Table VII. Computed wave parameters for internal wave train of 19 June 1976.

	$k = 2\pi/\lambda$ (meters^{-1})	C_i (m/sec)	$L = C_i T$ (km)	$L/(2\Delta H)$
$C_i = \omega/k \cong \frac{(\Delta p)}{\rho(\Delta u)}$		2.	1.3	10.
Two-Layer Model				
$C_i^2 \cong gh\Delta \ln\theta$		11.	6.7	54.
Three-Layer Model				
Fundamental	1.1×10^{-3}	9.	5.6	45.
2nd Harmonic	6.5×10^{-3}	1.5	1.	8.

$(2\Delta H)$ = transition layer thickness = 124m.

Observed period of 5.5-hour wave train = 600-660 secs.

Observed microbarograph pressure crests (measured from running mean) $\leq$ 55 μbars (except for one point); the crests are modulated at a 41-minute periodicity.

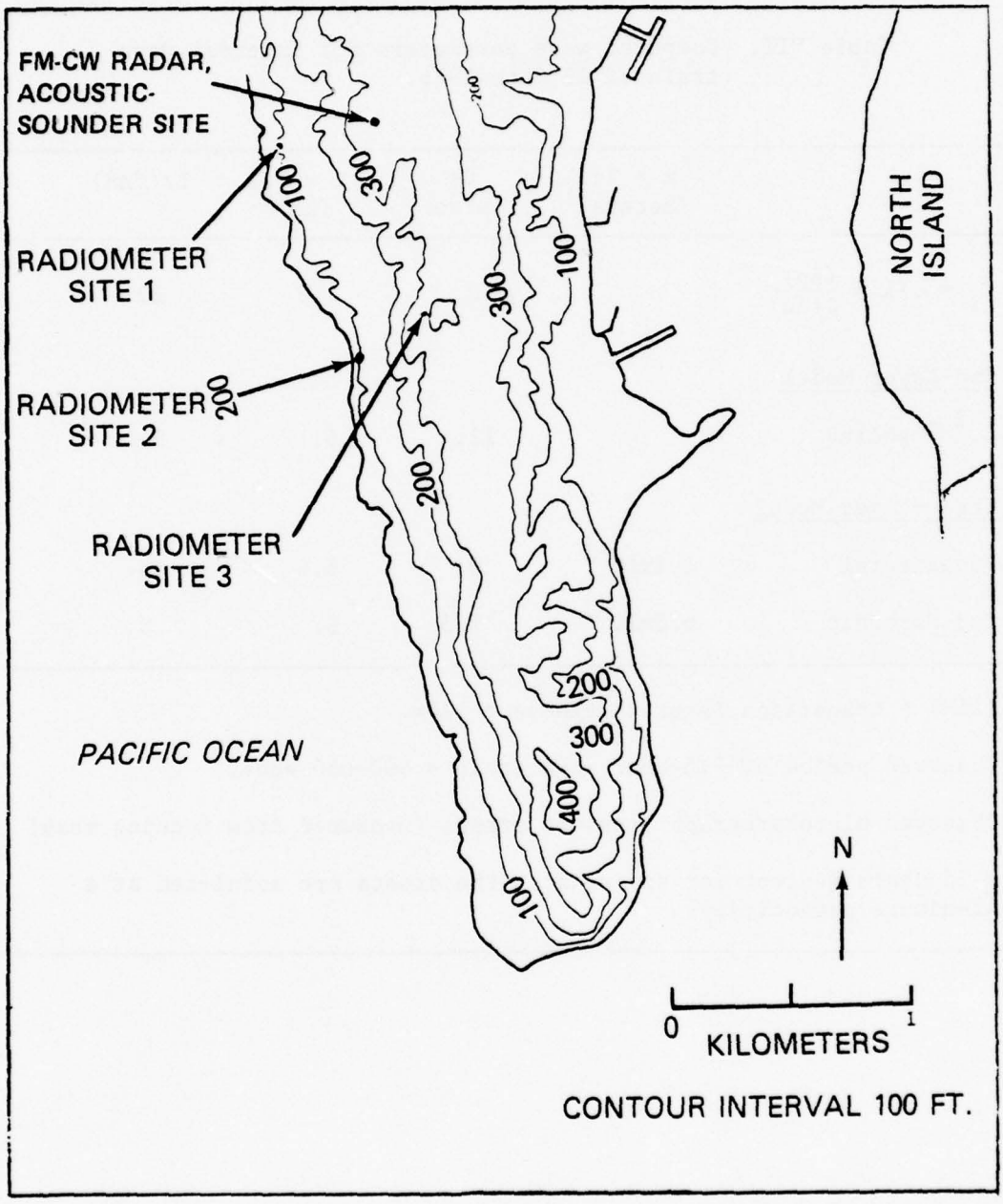

Fig. 1 - Topographic map of Pt. Loma Peninsula in San Diego, California, showing location of equipment for detection of internal waves.

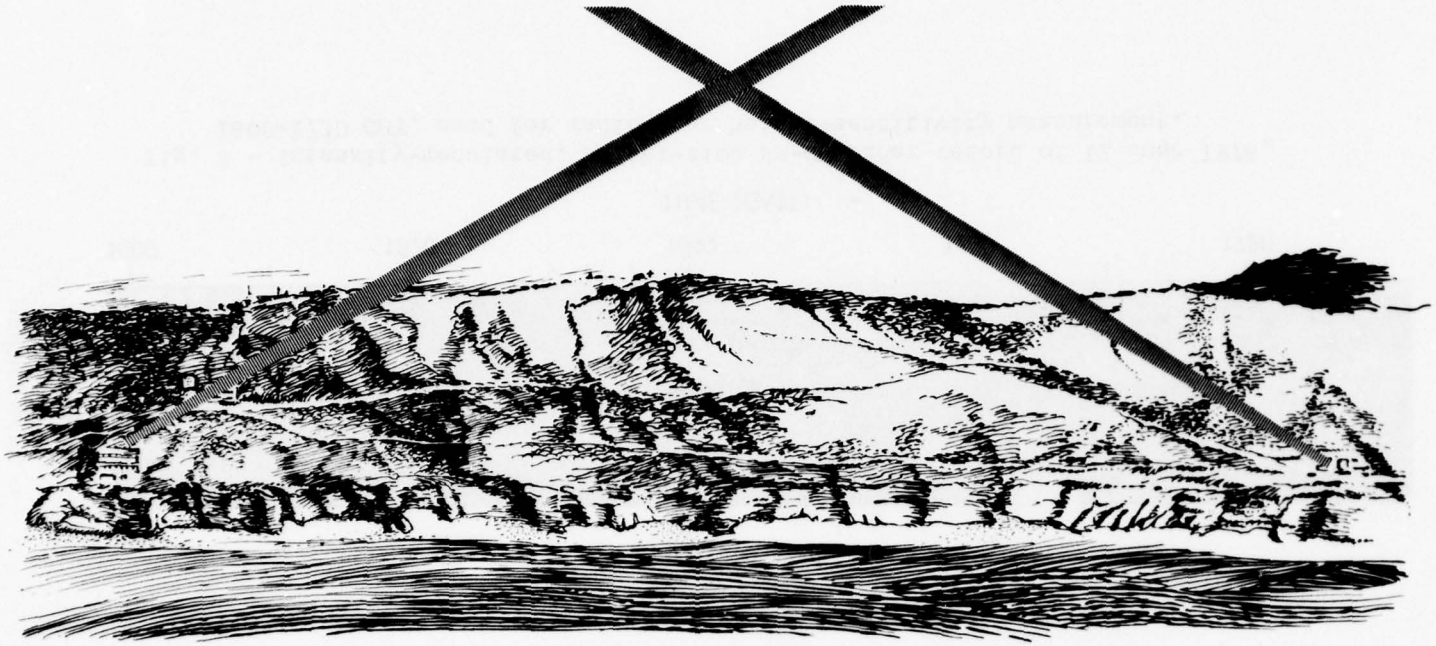

Fig. 2 - North-South sketch of Pt. Loma Peninsula, San Diego, California, showing final locations (sites S_1 and S_2) of 3^o beamwidth, 22 GHz radiometers used in marine boundary-layer experiment.

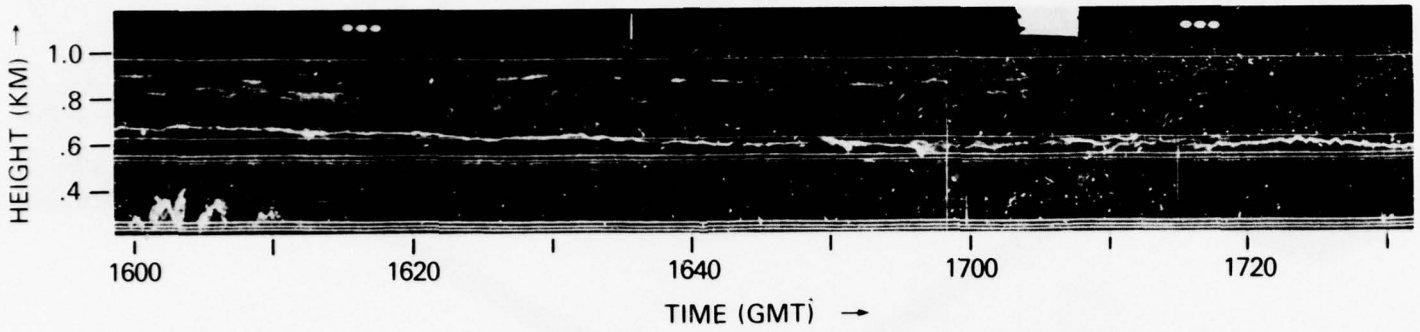

Fig. 3 - Intensity-modulated, height-time FM-CW radar record of 12 June 1976, 1600-1730 GMT, used for radiometer height-sensitivity measurement.

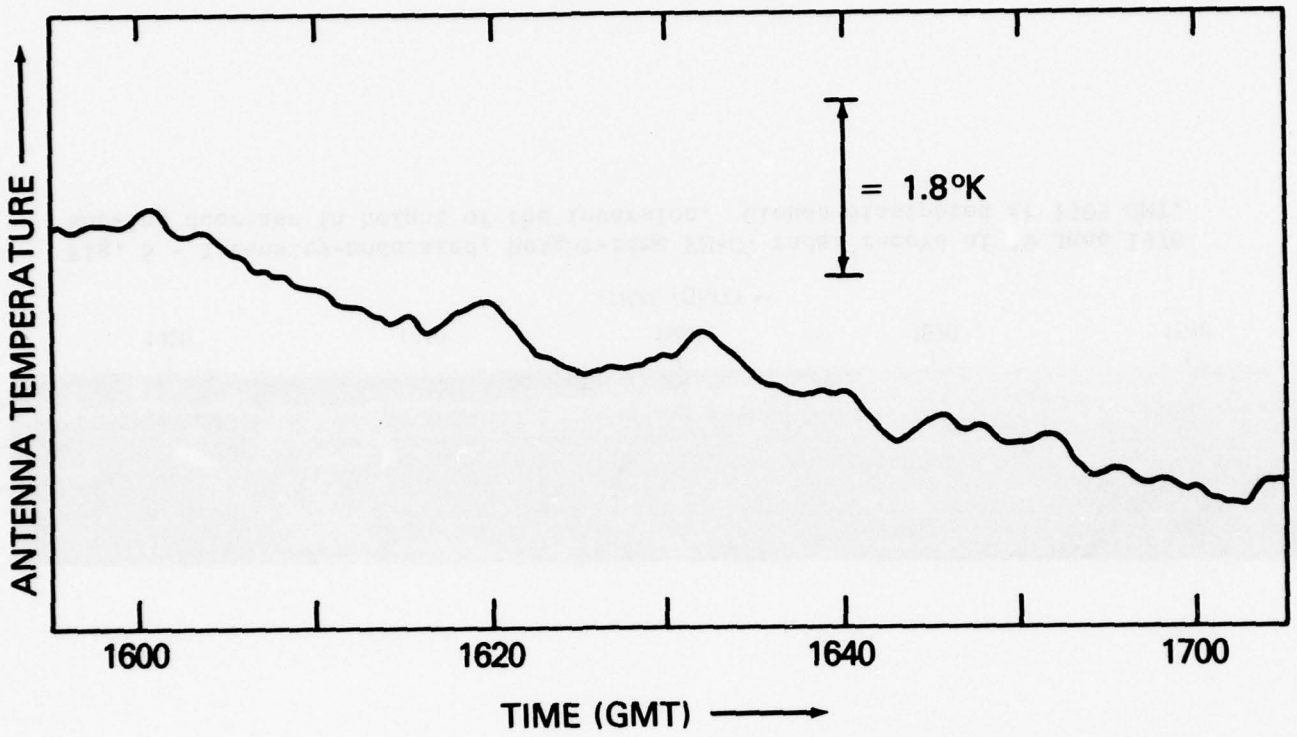

Fig. 4 - Signal of S_3 radiometer versus time on 12 June 1976 showing temperature decrease corresponding to 100-meter decrease in altitude of inversion base. Radiometer elevation angle = 60^{o}.

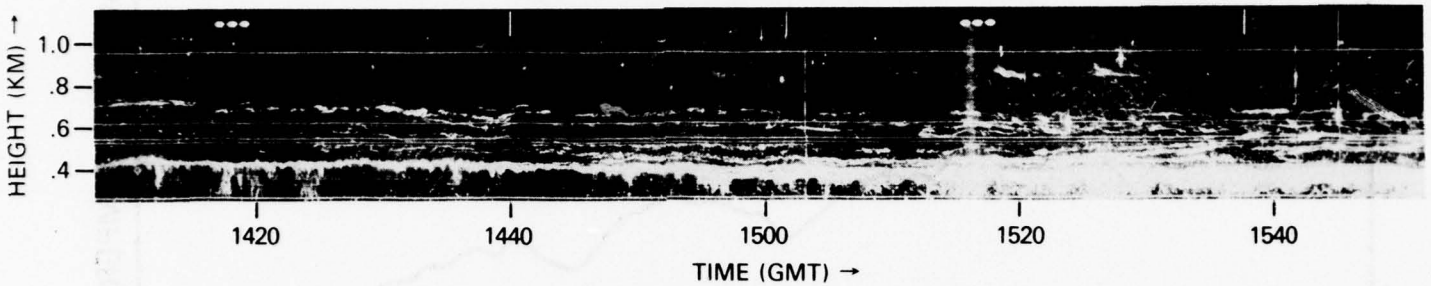

Fig. 5 - Intensity-modulated, height-time FM-CW radar record of 19 June 1976 showing decrease in height of the inversion. Clouds dissipated at 1503 GMT.

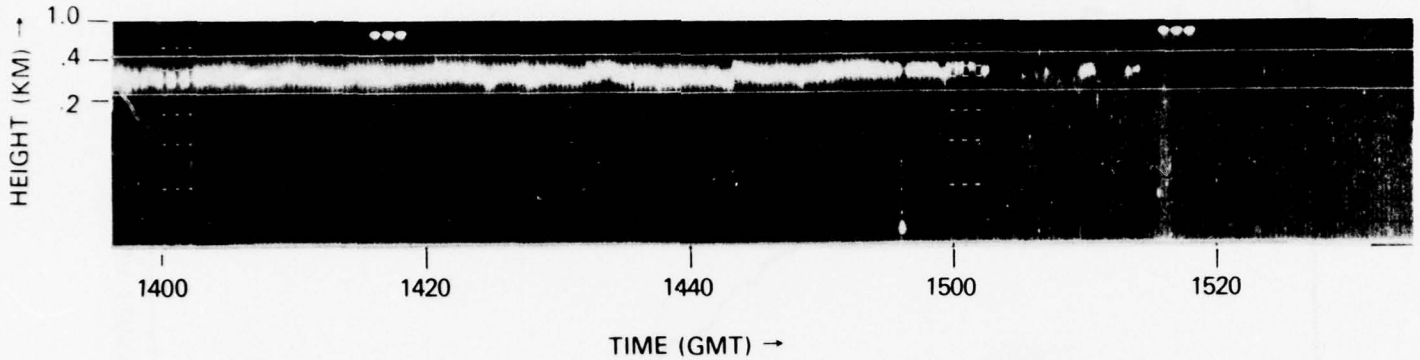

Fig. 6 - Height-time ceilometer record of 19 June 1976, 1400-1550 GMT showing sudden breakup of cloud layer at 1503 GMT during decrease in height of inversion.

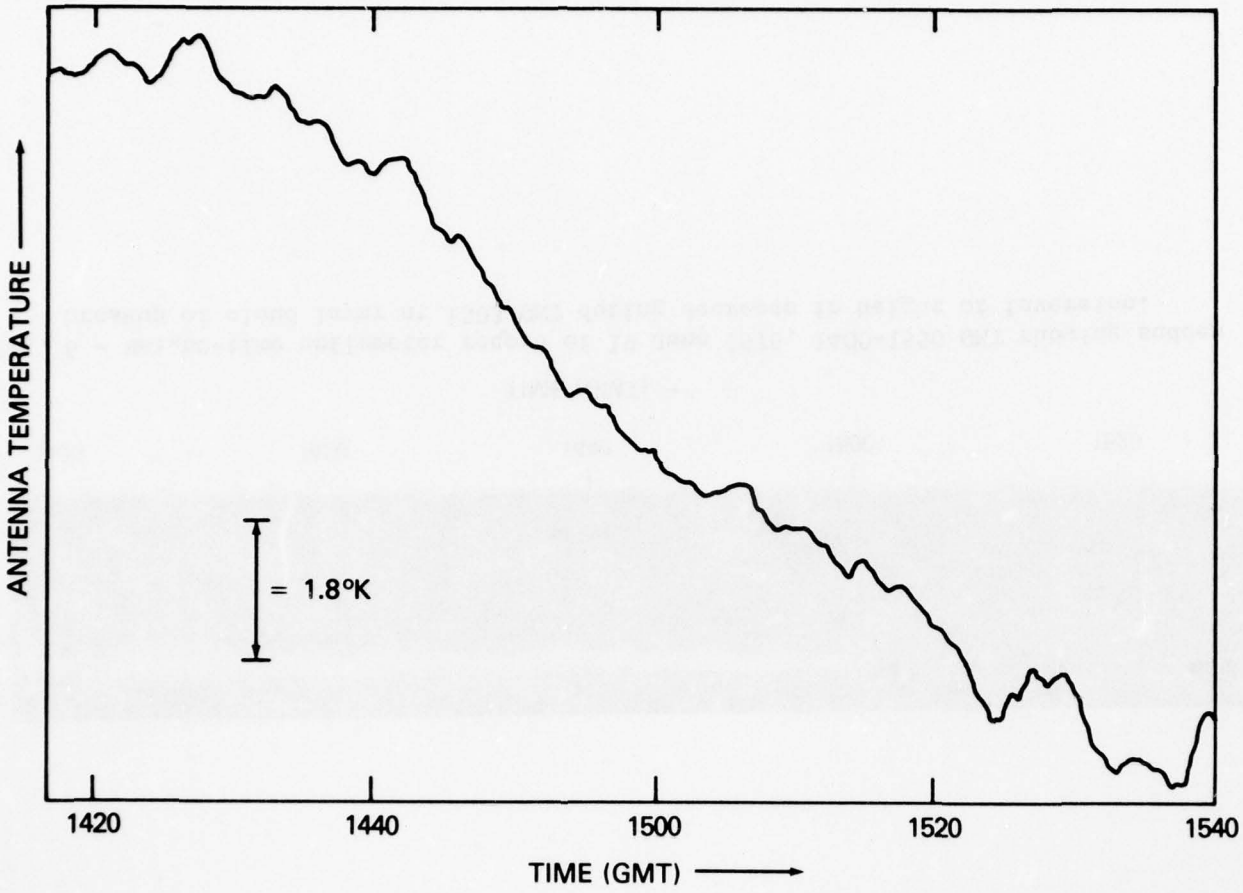

Fig. 7 - Signal of S_2 radiometer versus time on 19 June 1976 during 70-meter decrease in height of inversion between 1430 and 1520 GMT. Skies changed from overcast to clear at 1503 GMT. Radiometer elevation angle = 35°.

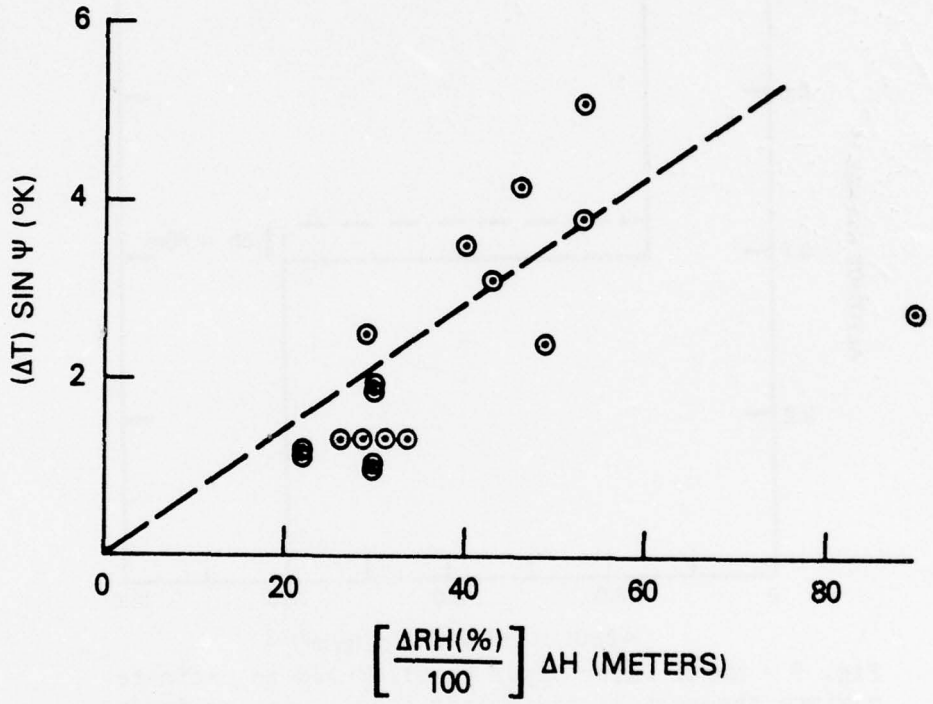

Fig. 8 - Radiometer height sensitivities, June 1976

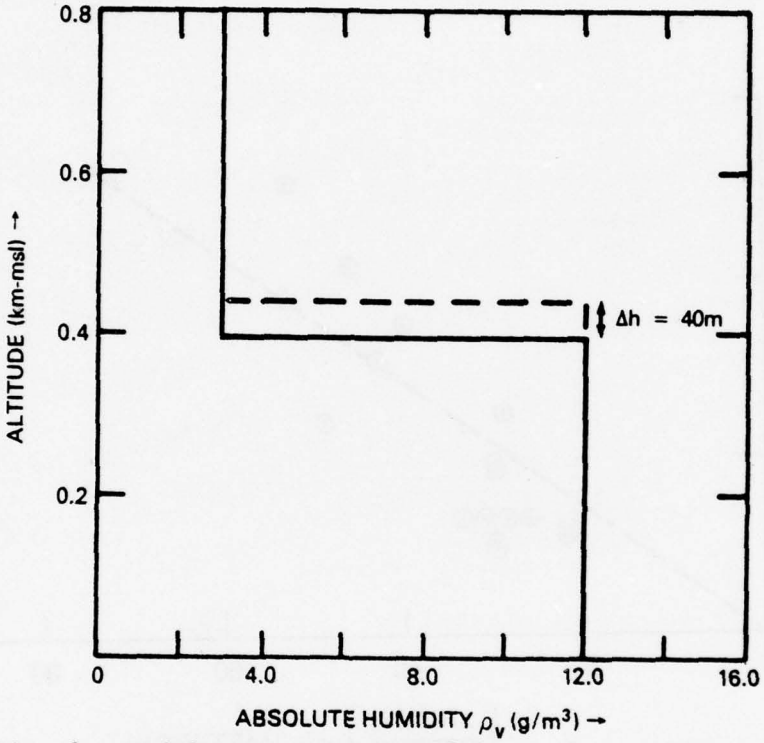

Fig. 9 - Model water vapor profile used to estimate maximum theoretical radiometer sensitivity to inversion height changes.

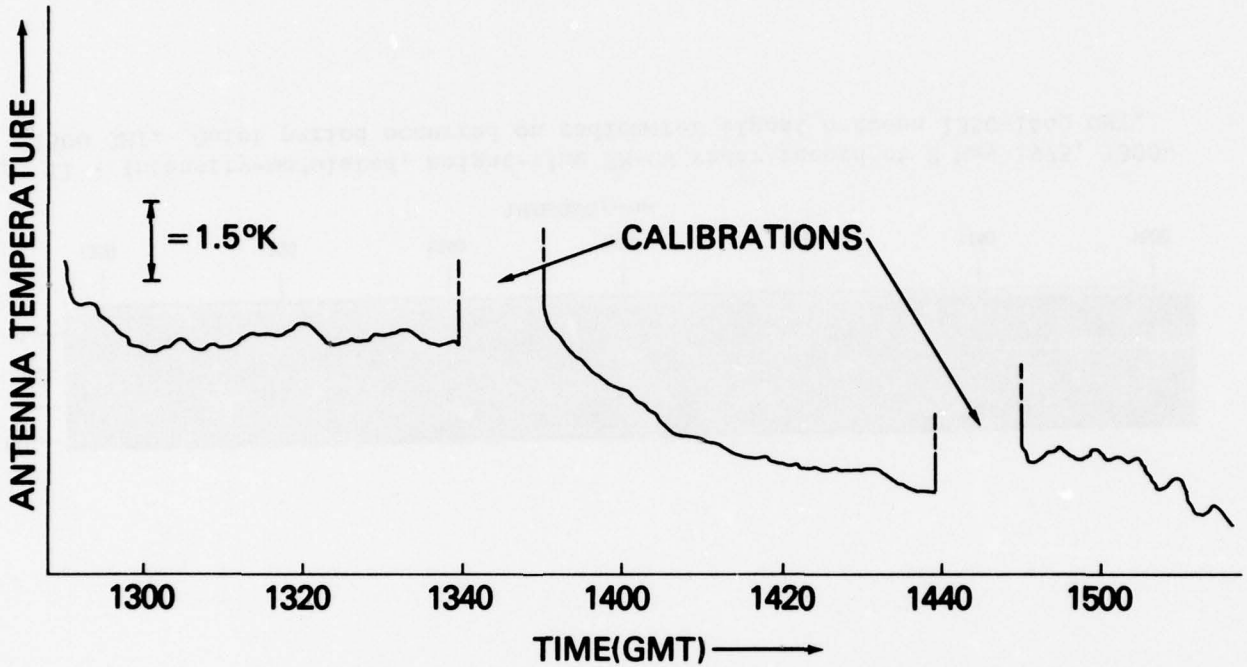

Fig. 10 - Signal of 3^{o} bw microwave radiometer versus time during quiet period on 8 May 1975. Elevation angle = 30^{o}.

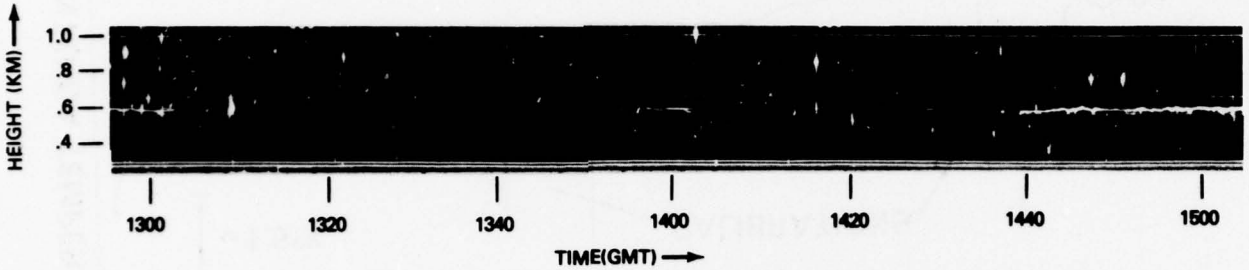

Fig. 11 - Intensity-modulated, height-time FM-CW radar record of 8 May 1975, 1300-1500 GMT. Quiet period occurred on radiometer signal between 1350-1440 GMT.

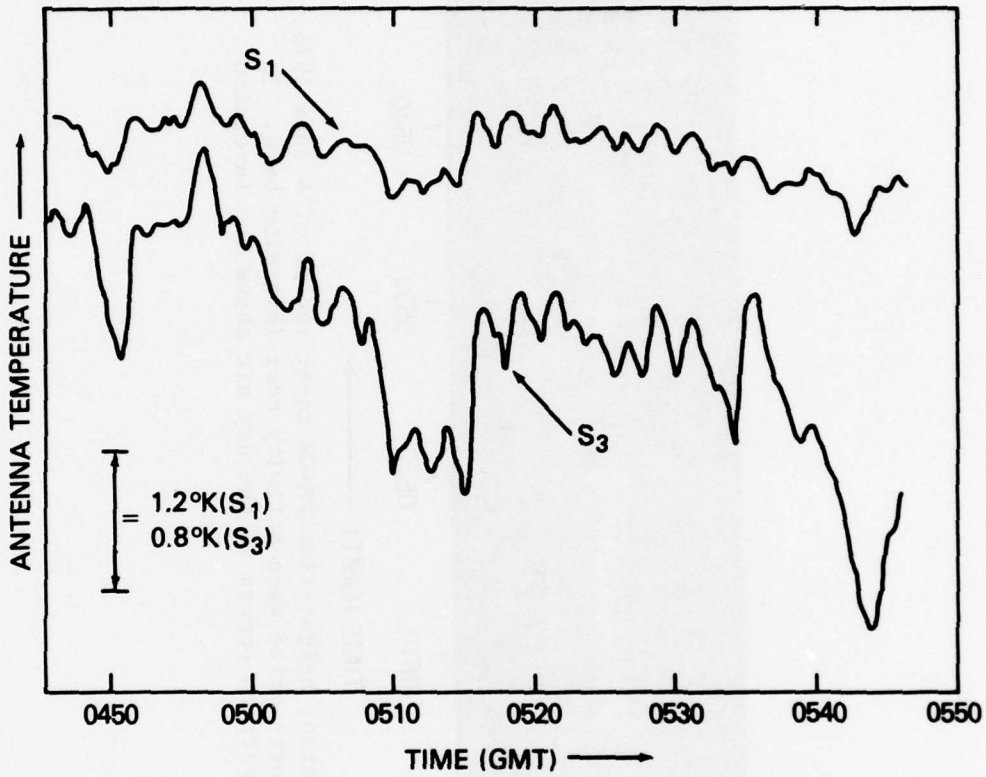

Fig. 12 - Correlated signals of S_1 and S_3 3° bw radiometers versus time for 4 June 1976 showing short-period waves between 0515-0540 GMT. Radiometer parameters are S_1 elevation = 56.5°, S_3 elevation = 52°. Radiometers pointed toward each other in azimuth.

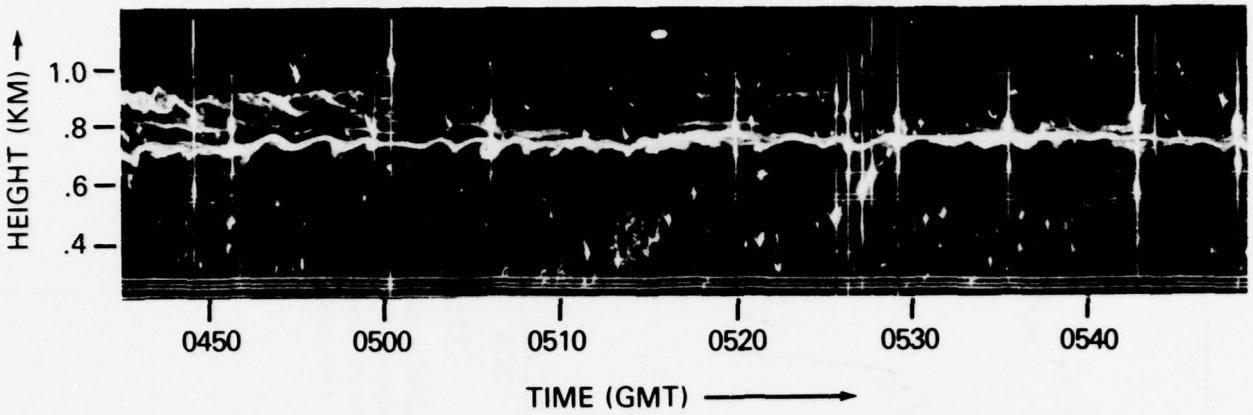

Fig. 13 - Intensity-modulated, height-time FM-CW radar record of 4 June 1976, 0445-0550 GMT, showing short-period wave activity near inversion base. In addition, a braided echo pattern occurs in the dry air above the inversion near 0445 GMT.

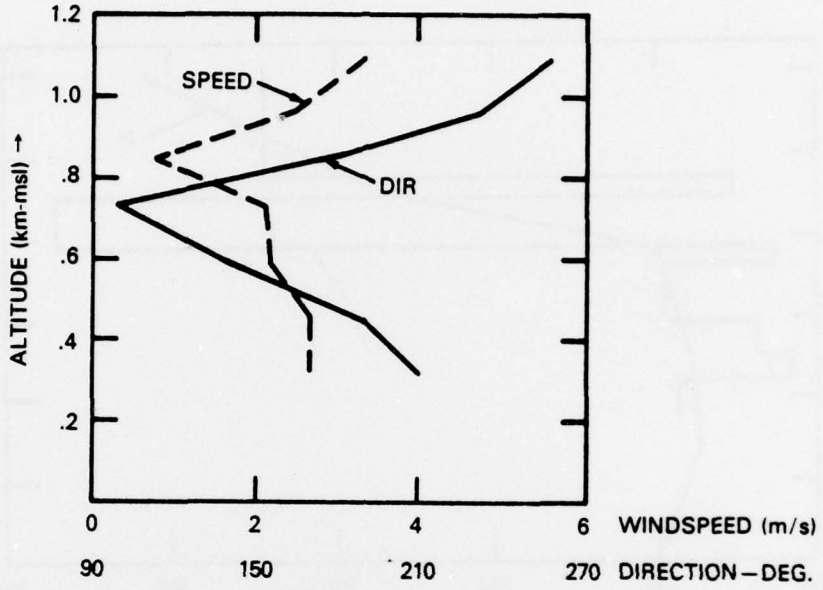

Fig. 14 - Wind speed and direction versus altitude from NOSC radiosonde at 1600 GMT on 4 June 1976.

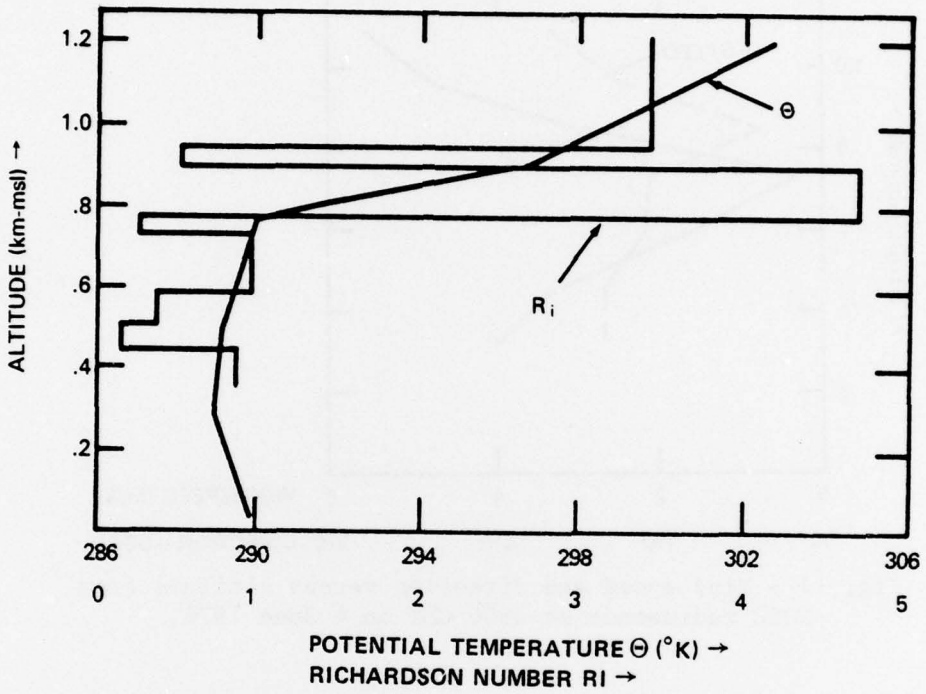

Fig. 15 - Potential temperature and Richardson's number versus altitude from NOSC radiosonde at 1600 GMT on 4 June 1976.

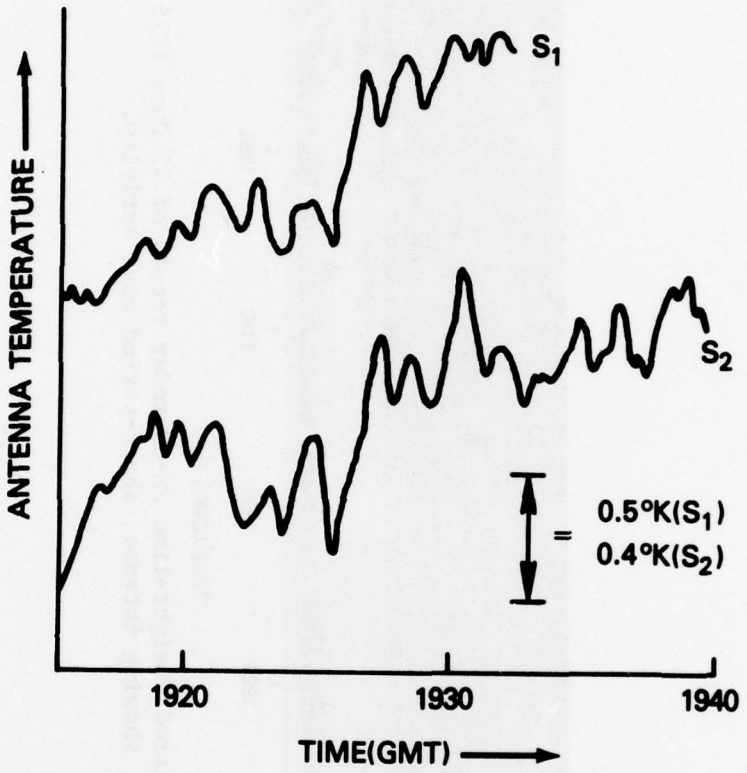

Fig. 16 - Singals of S_1 and S_2 3^o bw radiometers versus time for 17 June 1976 showing short-period wave activity between 1918-1932 GMT. Radiometer elevation angles = 45^o. Radiometers pointed toward each other in azimuth.

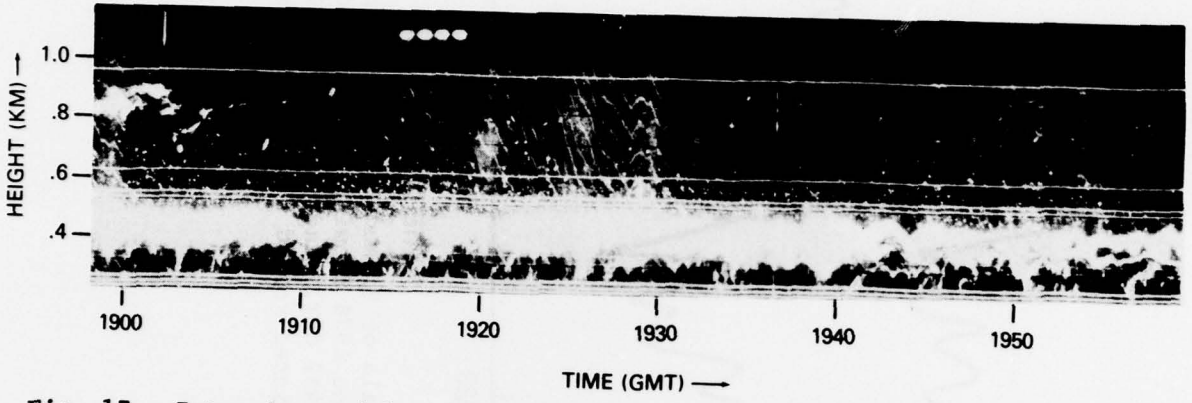

Fig. 17 - Intensity-modulated, height-time FM-CW radar record of 17 June 1976, 1900-2000 GMT, showing intense, short-period wave activity.

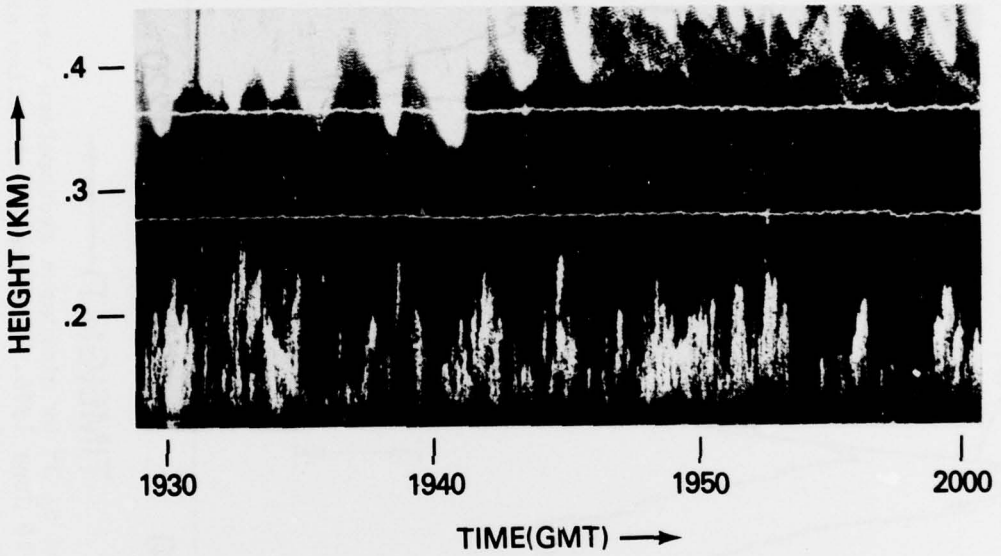

Fig. 18 - Intensity-modulated, height-time acoustic sounder record of 17 June 1976, 1930-2000 GMT, showing intense, short-period wave activity.

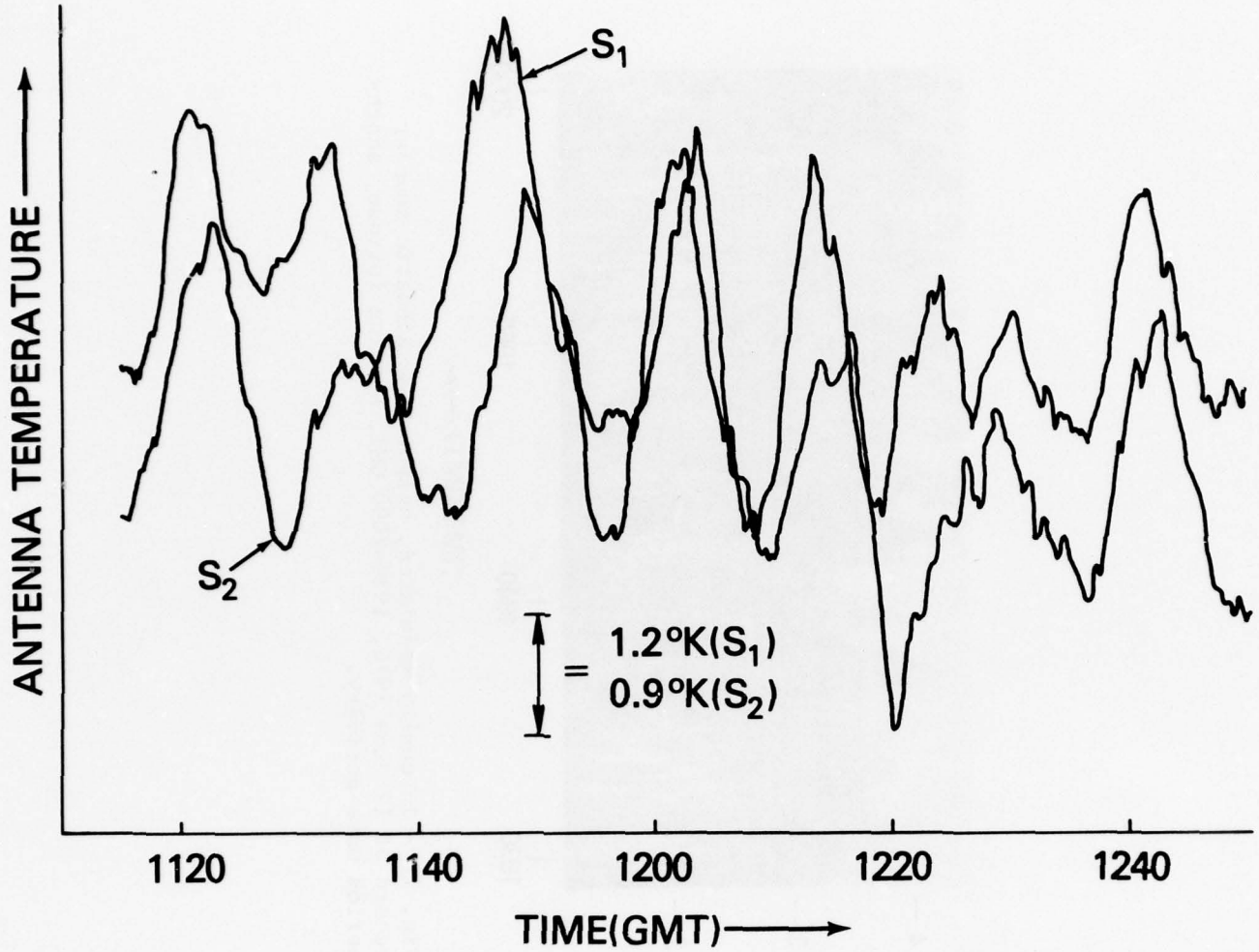

Fig. 19 - Signals of S_1 and S_2 3° bw microwave radiometers versus time during internal wave activity on 19 June 1976. Radiometer elevation angles = 35°. Radiometers pointed toward each other in azimuth.

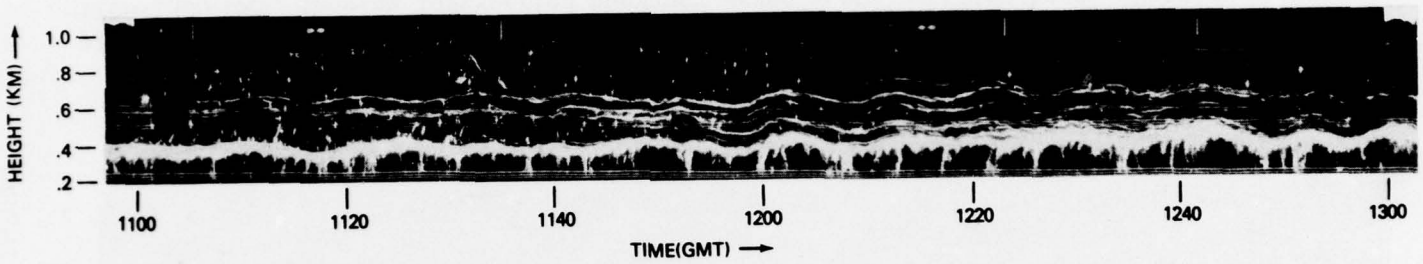

Fig. 20 - Intensity-modulated, height-time FM-CW radar record of 19 June 1976, 1100-1300 GMT, showing long-period buoyancy waves near inversion base. Multi-layered echoes in the dry air above inversion occur both in phase and out of phase with the primary waves below.

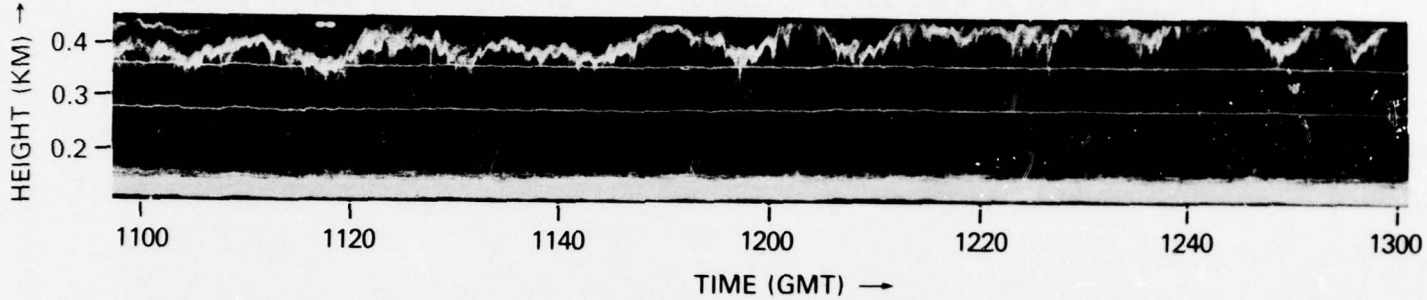

Fig. 21 - Intensity-modulated, height-time acoustic sounder record of 19 June 1976, 1100-1300 GMT, showing long-period buoyancy waves near inversion base. Short-period phenomena (possible convective activity) appear to be perturbing the long-period waves.

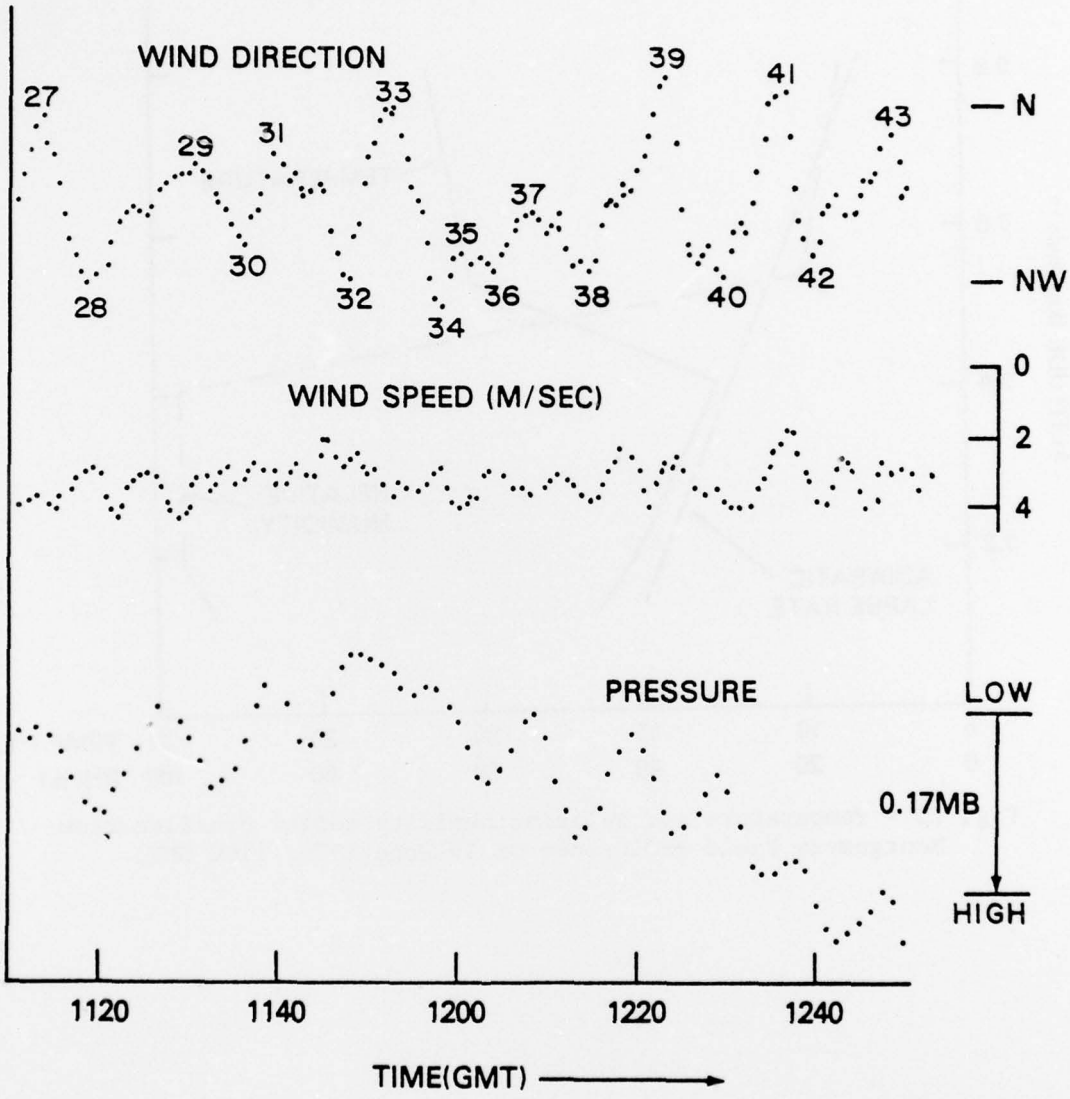

Fig. 22 - Surface meteorological records during internal wave activity on 19 June 1976.

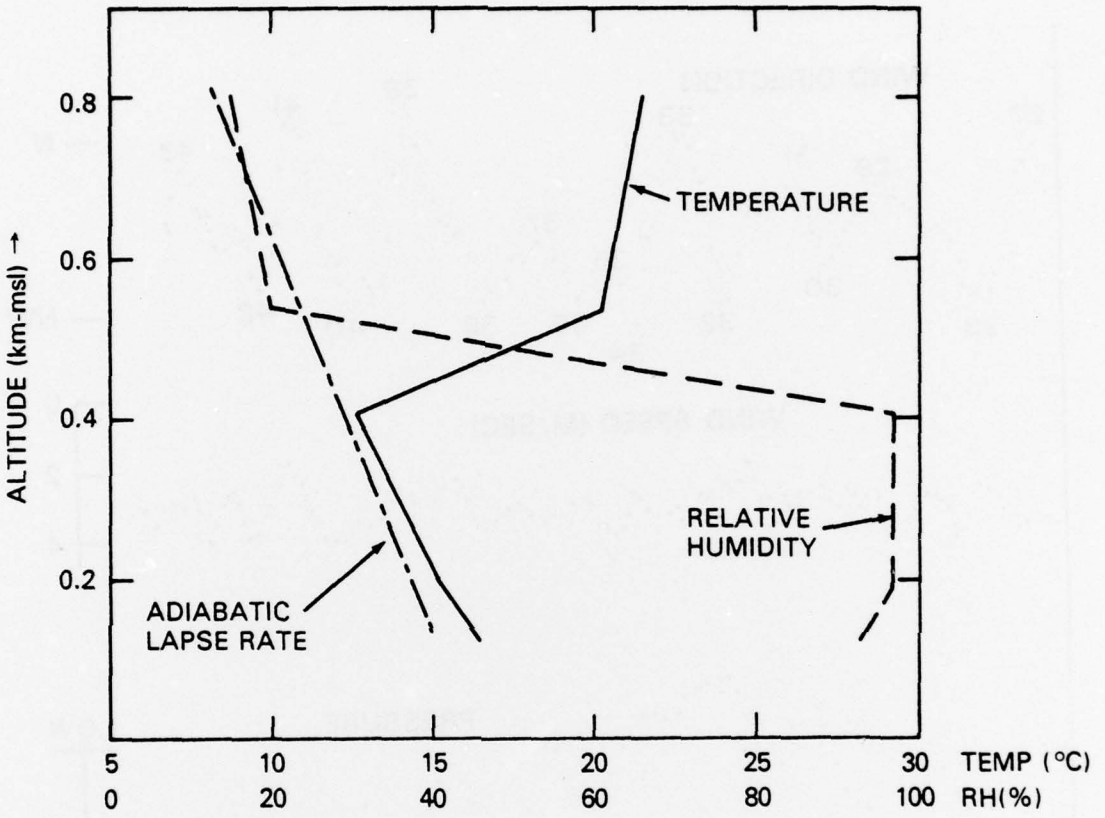

Fig. 23 - Temperature and relative humidity height profiles from Montgomery Field radiosonde on 19 June 1976, 1100 GMT.

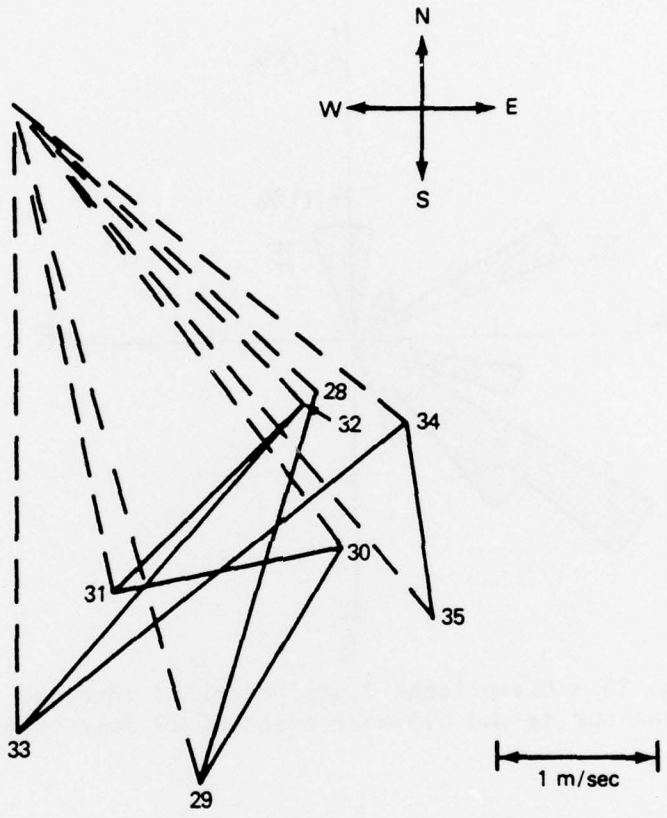

Fig. 24 - Construction of wind perturbation velocities for a portion of the wave train on 19 June 1976 (see text).

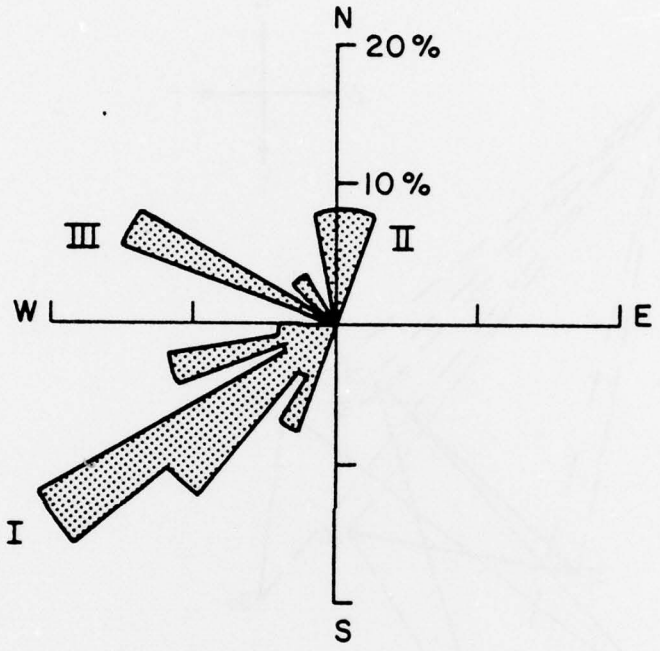

Fig. 25 - Directional distribution of internal waves during the 5.5-hour event of 19 June 1976.

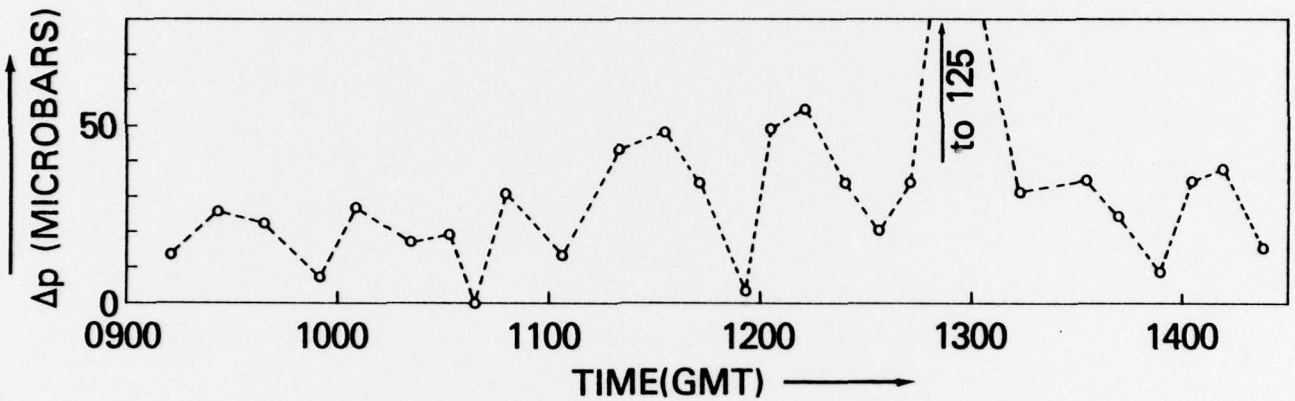

Fig. 26 - Observed microbarograph pressure crests measured from running mean during wave activity on 19 June 1976.

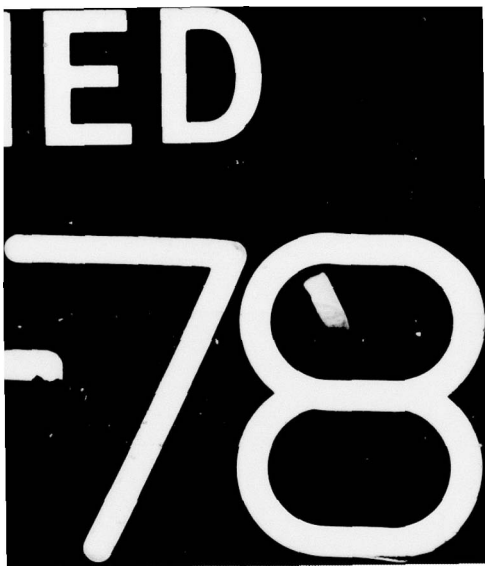
ED
78